Surface Soil Moisture Estimation Using Visible Light Polarimetry

Karen Aguilar

A thesis

submitted in partial fulfillment of the

requirements for the degree of

Master of Science in Electrical Engineering

University of Washington

2025

Committee:

Akshay Gadre

Payman Arabshahi

Program Authorized to Offer Degree:

Electrical and Computer Engineering

University of Washington

Abstract

Surface Soil Moisture Estimation Using Visible Light Polarimetry

Karen Aguilar

Chair of the Supervisory Committee:
Akshay Gadre
Department of Electrical and Computer Engineering

Accurate soil moisture estimations are critical for agricultural and environmental monitoring. However, current methods rely on direct contact with the soil and can be invasive or limited in scalability. This work investigates a non-invasive optical approach using visible light polarimetry (VLP) to estimate soil moisture, expressed as volumetric water content (VWC). A polarization camera was used in a controlled lab setup to capture images of three soil types under polarized lighting. The degree and angle of linear polarization were extracted from these images and found to correlate with moisture changes. To account for variability across soil types, a convolutional neural network (CNN) was used to improve the accuracy of soil moisture sensing using VLP. This research contributes to the advancement of non-invasive soil moisture sensing techniques with potential deployment in real-world conditions to address the limitations of current methods.

ACKNOWLEDGEMENTS

I would like to extend my gratitude to my advisor, Dr. Akshay Gadre, for his advice and support throughout my research and thesis. I would also like to thank Dr. Payman Arabshahi for being part of my reading committee and for his time and feedback in reviewing my work. Lastly, a special thanks to NSF IUCRC Center for Soil Technologies (SoilTech) for their support throughout the development of this research and NEWT Lab for their advice along the way.

I want to thank my mom, Maria, and my siblings, Mikey and Tali, for their unwavering support, endless encouragement, and boundless love, which have been the foundation upon which I have built my dreams. Ma, your strength, sacrifices, and quiet resilience have carried me through even the hardest days. Mikey and Tali, your laughter, jokes, late-night pep talks, and constant belief in me reminded me of why I kept going. Each step of this journey was made possible because of the three of you. This work is a testament to the strength and unity of our family.

With all my love, Karen.

DEDICATION

To my family for their infinite support

their unconditional love

and their unwavering belief in me.

TABLE OF CONTENTS

LIST OF FIGURES 6

LIST OF TABLES 8

Chapter 1. INTRODUCTION 9

Chapter 2. MOTIVATION AND BACKGROUND 11

2.1 MOTIVATION 11

2.2 BACKGROUND 12

2.2.1 IMPORTANCE OF CORRECTION ALGORITHMS 12

2.2.2 PRINCIPLES OF POLARIZATION IN SOIL SENSING 13

2.2.3 DEEP LEARNING FOR POLARIMETRIC DATA 14

Chapter 3. RELATED WORK 14

3.1 SATELLITE REMOTE SENSING TECHNOLOGIES 14

3.2 WIRELESS SENSING NETWORKS IN AGRICULTURE 18

3.3 IN-SITU SOIL MONITORING TECHNIQUES 20

Chapter 4. OBJECTIVE AND APPROACH 22

4.1 OBJECTIVE 22

4.2 APPROACH 22

Chapter 5. ITERATIVE DESIGN AND SENSOR VALIDATION 25

5.1 EARLY SENSOR SELECTION AND EVALUATION 25

5.2 TRANSITION TO WIRELESS DATA LOGGER 26

5.3 GRAVIMETRIC ANALYSIS 27

5.4 SELECTION OF THE TEROS 10 IN-SITU MOISTURE SENSOR....28

Chapter 6. SENSING SYSTEM....29

6.1 DATA PREPROCESSING AND IMAGE AQUISITION....29

6.2 NETWORK ARCHITECTURE....30

6.3 TRAINING PROCESS....32

6.4 MODEL PERFORMANCE METRICS....32

Chapter 7. EXPERIMENTAL SETUP....33

Chapter 8. RESULTS....37

Chapter 9. DISCUSSION AND LIMITATIONS....51

Chapter 10. CONCLUSION....54

Chapter 11. FUTURE WORK....55

BIBLIOGRAPHY....58

LIST OF FIGURES

Figure 1. Simplified diagram of the final setup showing a camera angled at the soil, illuminated by a polarized LED ring. A soil moisture sensor provides ground-truth data, with all components connected to a computer..... 10

Figure 2. Traditional soil moisture measurement methods: in-situ sensing with a capacitance probe and gravimetric sampling in a lab setting. 11

Figure 3. A 4-pixel block allows for the detection of all linear angles of polarized light by comparing the rise and fall in intensities transmitted between each pixel in the 4-pixel block. 23

Figure 4. Light reflecting off a wet soil surface at Brewster's angle becomes polarized, enabling surface moisture detection through polarimetric imaging. 24

Figure 5. Early selection of SM sensors used for comparison. The Arduino capacitive sensor (far left), Adafruit STEMMA (second from left), ECOWITT wireless (center), and precision balance (right) used for gravimetric SM estimation. 26

Figure 6. A convolutional neural network architecture for estimating surface soil moisture from polarized 8-bit grayscale images. 31

Figure 7. Simplified diagram of the setup showing a camera angled at the soil, illuminated by a polarized LED ring. A soil moisture sensor provides ground-truth data, with all components connected to a computer. 34

Figure 8. Experimental setup showing a soil sample placed inside a box, illuminated by a ring light with a linear polarizer. A camera is angled through a top opening to capture polarized reflectance near Brewster's angle..... 35

Figure 9. Pixel formats captured by the Triton polarization camera on initially moist loamy soil. From left to right: PolarizeMono8, PolarizedDolp_BayerRG8, and PolarizedAolp_BayerRG8. 35

Figure 10. Three soil types used in experiments: (left) loamy soil, (center) organic-rich garden soil, and (right) sandy soil. Each differs in texture, composition, and moisture retention properties..... 37

Figure 11. Predicted and actual soil moisture (% VWC) over sample order in Cycle 1 for (a) training and (b) testing data. 39

Figure 12. Scatter plots comparing predicted and actual soil moisture values (% VWC) for (a) training and (b) testing datasets for Cycle 1. 40
Figure 13. Comparison of predicted and actual soil moisture values (% VWC) for (a) training and (b) testing data in Cycle 1. Each plot has a best-fit line (red) and a dotted ideal 1:1 reference line (black). 40
Figure 14. Predicted and actual soil moisture (% VWC) over sample order in Cycle 2 for (a) training and (b) testing data. 42
Figure 15. Scatter plots comparing predicted and actual soil moisture values (% VWC) for (a) training and (b) testing datasets for Cycle 2. 43
Figure 16. Comparison of predicted and actual soil moisture values (% VWC) for (a) training and (b) testing data in Cycle 2. Each plot has a best-fit line (red) and a dotted ideal 1:1 reference line (black). 43
Figure 17. Predicted and actual soil moisture (% VWC) over sample order in Cycle 3 for (a) training and (b) testing data. 46
Figure 18. Scatter plots comparing predicted and actual soil moisture values (% VWC) for (a) training and (b) testing datasets for Cycle 3. 47
Figure 19. Comparison of predicted and actual soil moisture values (% VWC) for (a) training and (b) testing data in Cycle 3. Each plot has a best-fit line (red) and a dotted ideal 1:1 reference line (black). 47
Figure 20. Predicted and actual soil moisture (% VWC) over sample order in Cycle 4 for (a) training and (b) testing data. 50
Figure 21. Scatter plots comparing predicted and actual soil moisture values (% VWC) for (a) training and (b) testing datasets for Cycle 4. 50
Figure 22. Comparison of predicted and actual soil moisture values (% VWC) for (a) training and (b) testing data in Cycle 4. Each plot has a best-fit line (red) and a dotted ideal 1:1 reference line (black). 51

LIST OF TABLES

Table 1. Average Training Performance Metrics of Soil Moisture Estimation with Different Soil Types. 44
Table 2. Average Testing Performance Metrics of Soil Moisture Estimation with Different Soil Types 44
Table 3. Average Training Performance on Two Consecutive Cycles with the Same Organic-Rich Soil. 48
Table 4. Average Testing Performance on Two Consecutive Cycles with the Same Organic-Rich Soil..... 48

Chapter 1. INTRODUCTION

Soil moisture dynamics are a critical factor in influencing agricultural productivity, environmental health, and water resource management [1]. Accurate and timely soil moisture measurement helps farmers make informed decisions about irrigation and fertilization practices, supporting sustainable land and water management. Traditional methods of measuring soil moisture, such as gravimetric analysis or sensors in the ground, can be accurate but are time-consuming and are limited to having direct contact with the soil. This constrains their practicality for large-scale or real-time applications [1, 2].

To overcome the limitations of in-ground soil moisture measurements, researchers have investigated remote sensing to collect soil moisture readings without contact with the ground [3, 4]. These methods can cover large areas quickly and are useful for real-time monitoring [2, 5-7]. One emerging method in this area is visible light polarimetry (VLP), a non-invasive technique for soil moisture sensing [8], with potential for integration alongside traditional SAR-based methods [9]. This approach utilizes the polarization properties of reflected light to infer soil moisture levels, providing the potential for fast and remote assessments in a proximal and scalable solution [2, 8, 10].

However, the effectiveness of polarimetric measurements can be significantly influenced by soil texture and moisture conditions, which determine the water-holding capacity and vary widely across different agricultural and environmental settings. Soil textures can be categorized into different types, such as sandy, loamy, and organic-rich, which affect the scattering and absorption of light. These differences can alter the polarization characteristics of reflected light, presenting a challenge for accurate moisture estimations [4, 7].

This work presents how VLP can be used to estimate soil moisture across different soil types and introduces correction methods to improve prediction accuracy under varying surface conditions. The study was conducted in controlled laboratory experiments to analyze how varying soil textures and moisture levels influence the polarization properties of reflected light at the surface (0-5cm) level of soil moisture. The overall system seen in Figure 1 had some early challenges with factors such as sensor selections and ambient lighting conditions affecting the images, soil surface roughness, and variability within soil samples, which required careful management throughout the experiments. Addressing these challenges also created new opportunities for future research to develop correction algorithms that can be tested under real-world conditions, thereby transitioning from controlled lab experiments to outdoor field tests. Additionally, integrating these methods with existing satellite-based SAR systems can improve large-scale soil moisture monitoring for sustainable water management.

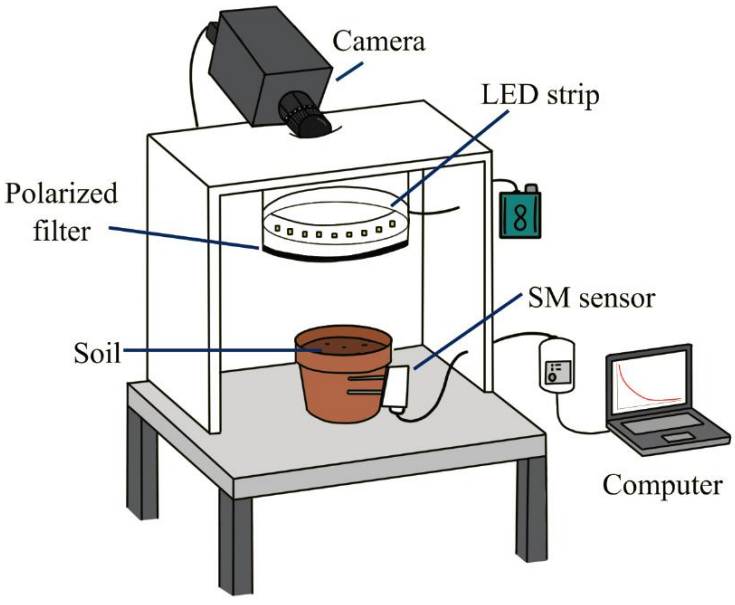

Figure 1. Simplified diagram of the final setup showing a camera angled at the soil, illuminated by a polarized LED ring. A soil moisture sensor provides ground-truth data, with all components connected to a computer.

The significance of this research lies in its potential to advance non-invasive soil moisture measurement techniques. By addressing the variability introduced by different soil types, this work supports the applicability of VLP as a contact-free tool for monitoring soil moisture, offering practical value to farmers, researchers, and environmental managers [1, 2].

Chapter 2. MOTIVATION AND BACKGROUND

2.1 MOTIVATION

Many farmers and environmental managers rely on accurate information on soil moisture to make informed decisions about irrigation, crop health, and sustainable resource use. However, traditional methods for measuring surface soil moisture (upper 0-5 cm topsoil layer), such as gravimetric sampling or in-situ capacitive sensors, can be time-consuming, requiring extensive calibration, or lack durability (see Figure 2) making them difficult to scale for real-time field applications [11-14].

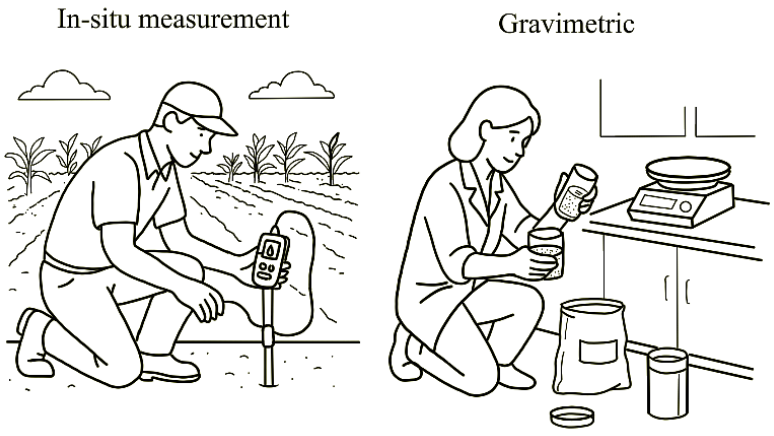

Figure 2. Traditional soil moisture measurement methods: in-situ sensing with a capacitance probe and gravimetric sampling in a lab setting.

For scalable alternatives, remote sensing technologies, such as synthetic aperture radar (SAR) and satellite-based optical imaging (e.g., Sentinel-1 and Sentinel-2 missions) [15-18] can provide spatial coverage. While SAR and satellite techniques can provide wide coverage, they are sensitive to surface roughness and dense vegetation, requiring complex modeling and often lacking the resolution necessary for smaller field-scale soil monitoring [9, 19].

An emerging alternative is visible-light polarimetry**,** a non-contact optical approach that uses the polarization of reflected light quantified as the Degree of Linear Polarization (DoLP) and Angle of Linear Polarization (AoLP) to gather surface characteristics, including soil moisture [8, 20-22]. This method holds promise for fast, low-cost, and deployable field sensing. However, its effectiveness is significantly influenced by the amount of water in the soil, and how the surface changes, which affects the reflectance and scattering behavior depending on particle size and mineral composition [21-23].

2.2 BACKGROUND

2.2.1 *IMPORTANCE OF CORRECTION ALGORITHMS*

The importance of algorithms to address the variability introduced by different soil types is high, as they can adjust polarimetric readings based on underlying soil properties [23, 24]. These corrections can provide passive sensing products with a more reliable estimation across moisture and lighting conditions. Similar correction methods are used in other remote sensing domains. For example, in microwave-based GNSS reflectometry, systems like CYGNSS apply Fresnel reflection and water content corrections to improve the accuracy of soil moisture readings [25]. For a physics-informed correction strategy, visible-light polarimetry has shown potential as a

non-contact method for estimating surface soil moisture because of its sensitivity to visual changes, making it ideal for high-resolution soil monitoring.

2.2.2 *PRINCIPLES OF POLARIZATION IN SOIL SENSING*

Polarimetry refers to the measurement of the polarization state of light, which can help measure soil moisture effectively due to the way moist soil alters light reflection and scattering. When polarized or unpolarized incident light strikes a soil surface, the reflected light becomes partially polarized depending on the surface characteristics [26]. The presence of water on the soil surface greatly influences this polarization effect by altering the refracted indices between water and soil particles, leading to measurable changes in the polarization state of the reflected light [27].

When soil becomes moist, the water binds to the soil particles, modifying the surface texture, which affects the reflectance and scattering behavior of light [27]. Additionally, moisture affects the dielectric properties of the soil, affecting how the incident light scatters when interacting with the surface and modifying the polarization state and intensity of the reflected light [21, 22]. These changes are prominent at the surface level, where evaporation and infiltration occur rapidly, making VLP sensitive to moisture-related surface dynamics [28].

The commonly used descriptors in polarimetric imaging are the degree of linear polarization (DoLP) and the angle of linear polarization (AoLP). DoLP represents the magnitude of how much of the reflected light is linearly polarized, and AoLP indicates the direction of that polarization [29]. Both values vary depending on the soil's moisture level [22, 26]. In dry soil, the polarization tends to be stronger due to the less water absorption and stronger reflection of light, leading to a higher DoLP. In contrast, moist soil increases absorption and changes the refractive properties of the surface, which reduces the overall polarization and lowers DoLP. Similarly, dry soil surfaces reflect light in a more consistent manner, allowing for clearer

estimation of AoLP. However, as moisture increases and scattering occurs, the direction of the reflected light becomes less predictable and the AoLP measurements are more variable. Due to its sensitivity to subtle surface changes, VLP offers a valuable method for non-invasive, high-resolution soil moisture monitoring. Previous studies have demonstrated that VLP can capture reflectance patterns related to moisture in the upper soil layer [8, 28, 30], making it suitable for detecting early shifts in surface moisture content.

2.2.3 *DEEP LEARNING FOR POLARIMETRIC DATA*

While VLP provides important image data, interpreting polarization patterns across varying soil types can be difficult. Deep learning models, such as convolutional neural networks (CNNs)**,** have shown significant promise in soil moisture prediction from image-based data [17, 31-33]. CNNs can extract subtle spatial and textural patterns that are often difficult to capture through manual feature design [34, 35]. It has been successfully applied in soil moisture prediction from satellites and imaging radars [3, 36]. This makes the CNN an effective method for learning from the reflectance and polarization features captured in polarized images.

Chapter 3. RELATED WORK

This section provides a comprehensive review of related work in agricultural sensing, including satellite-based remote sensing, wireless sensor networks, and in-situ measurement techniques.

3.1 SATELLITE REMOTE SENSING TECHNOLOGIES

Satellite soil moisture retrievals are generally produced at a spatial resolution on the order of kilometers, which introduces uncertainty when trying to capture the small-scale spatial heterogeneity of land surfaces [37]. To solve this uncertainty, many researchers propose

downscaling retrievals to a more appropriate level [37]. Much focus has been on passive microwave methods, especially missions such as the Soil Moisture and Ocean Salinity (SMOS) satellite launched by the European Space Agency in 2009, that uses a 1.4 GHz L-band radiometer to provide global measurements of soil moisture and ocean salinity. Additionally, NASA launched the Soil Moisture Active Passive (SMAP) radar in 2015 which was designed to combine both active (radar, 1.26GHz) and passive (radiometer, 1.4 GHz) [37]. SMAP captures images of the Earth every 2-3 days to estimate soil moisture. However, SMAP often relies on readily available visible-near infrared and thermal observations, using surface temperature and vegetation parameters to help constrain the soil moisture estimates. These products are usually validated using a mix of core-monitoring sites, field campaigns, and multi-satellite comparisons [37-40].

An additional factor to consider regarding soil moisture is reflectance; the sunlight that "bounces" back from the Earth's surface decreases as soil moisture increases. Some studies have even found a linear relationship between water absorption bands and soil water content, but these empirical approaches often perform poorly since reflectance is also influenced by attributes such as soil texture, mineral content, surface roughness, and organic matter [38]. While remote sensing still depends on in-situ measurements, it has limitations. For example, shallow soil penetration and dense cloud coverage continue to be significant issues [37, 38, 40]. The two primary types of retrieval methods are statistical approaches, which involve regressing brightness temperature against measured soil moisture, and forward model inversion techniques. The lower frequency microwave bands (1–3 GHz) have solid physical backing for measuring soil moisture, especially the L-band, which can penetrate most types of vegetation cover [38]. However, long wavelengths mean large antennas, which are challenging to place into orbit due to size and cost

constraints. Also, most current algorithms only work well for flat, weakly vegetated areas. While backscattering models tend to work best for bare soil conditions, their accuracy significantly decreases on surfaces with vegetation due to the increased signal attenuation and surface scattering [38].

In another approach, rather than trying to measure rainfall directly, researchers reversed the problem and used changes in soil moisture to deduce how much rain had fallen, essentially using the soil as a natural rain gauge [39]. This "bottom-up" method uses variations in satellite-observed soil moisture after rainfall events to estimate prior rainfall amounts. Data from multiple satellites, including an Advanced Scatterometer (ASCAT), Advanced Microwave Scanning Radiometer-EOS (AMSR-E), and SMOS, were used to generate new daily rainfall products [39]. Specifically, the proposed Soil Moisture to Rain (SM2RAIN) algorithm is based on inverting the soil water balance equation to retrieve rainfall [39]. It performs well at large scales, even globally, but it tends to underestimate light rainfall events. This is why ground rain gauges and radar are still widely used. Additionally, dense vegetation like tropical forests limits satellite penetration, resulting in low accuracy in those regions. However, with an initial guess from real-time rainfall products like Tropical Rainfall Measuring Mission Multi-Satellite Precipitation Analysis (TMPA), the SM2RAIN framework can effectively correct and improve rainfall estimates [39].

In regard to validating satellite soil moisture products, it's not a straightforward process. Early applications focused on large-scale soil moisture dynamics using aircraft, but eventually evolved into satellite-linked experiments, split into pre- and post-launch phases [40]. Many experiments included labor-intensive fieldwork, later supported by long-term monitoring stations. Because in-situ data can be sparse or unrepresentative, researchers also use land surface

models (LSMs) as a reference, even though those models have their own uncertainties. This complicates identifying whether discrepancies arise from the satellite retrievals or the models. Additionally, various satellites utilize different wavelengths, polarizations, and angles, allowing them to detect varying soil depths. Satellite data rarely align with ground truth data in space or time, leading to representativeness errors. To mitigate these, preprocessing steps are implemented, such as masking out satellite retrievals defined for quality issues or using ancillary data to eliminate areas with forests, snow, wetlands, or cold surface temperatures below 4 °C [3, 18, 38-42]. Also, because time-of-day temperature gradients influence passive systems, retrieval quality can vary depending on when the observation is made. Most validation studies assume errors are random and have zero mean, which considers systematic additive or multiplicative biases. Satellite sensors are limited to detecting moisture within only the top few centimeters of soil [40]. Therefore, in-situ validation sensors or modeled soil layers should be constrained to depths no greater than 5-10 cm to ensure consistency with the satellite measurements [40].

Looking at more localized applications, researchers studying satellite-based soil moisture retrievals in places like Illinois found that even state-of-the-art systems like SMAP and SMOS come with trade-offs [41]. Passive microwave data from SMAP, for instance, works well for the top 5 cm soil layers and does better under low-vegetation conditions, but has poor performance in forested or rugged regions. Despite high revisit times and globally available datasets, retrieval accuracy can be undermined by surface roughness, vegetation structure, and frozen or snow-covered soils [41]. As a result, SMAP products tend to perform better in agricultural plains than in more heterogeneous landscapes [41].

Finally, combining ground, proximal, and satellite sensing has been key to better understanding soil moisture dynamics. While satellite sensors offer large-scale observations, they

still suffer from scale mismatches and sensor depth disparities compared to ground-based measurements. Newer efforts aim to refine validation methods by building standardized protocols that consider these mismatches. For example, integrating an Unmanned Aerial Vehicle (UAV) data with hyperspectral imaging has shown promise in bridging the resolution gap [43], though more work is needed to generalize these techniques across different soil and vegetation types. SMAP has shown consistent accuracy at its target threshold (0.04 cm^3/cm^3 RMSE), but performance varies significantly with land cover and seasonality [40]. Networks like the U.S. Drought Monitor are now incorporating satellite soil moisture estimates to support national-scale drought assessments, showing the growing operational value of these systems [37, 39, 41, 42].

3.2 WIRELESS SENSING NETWORKS IN AGRICULTURE

Wireless sensor networks (WSNs) have been a significant focus on soil moisture monitoring because they provide continuous, real-time, in situ data under various environmental conditions [44]. In one system, a WSN was deployed across three different crop fields (corn, cotton, soybean) using soil moisture and weather sensors at three depths to support irrigation scheduling [44]. The setup included Decagon sensors, from Decagon Devices (now known as METER), and Em50G/Em50R data loggers, which collected data every minute and averaged it hourly. The antennas had to be raised above the plant canopy to maintain signal strength, especially as the crop grew taller and the canopy interfered with Received Signal Strength Indicator (RSSI) values. This real-world deployment revealed common issues like animal damage to cables and the need to reset the loggers after thunderstorms occasionally [44].

Another study, conducted in an apple orchard, deployed 135 soil moisture sensors and 27 temperature sensors across 27 nodes, emphasizing the importance of maintaining a constant voltage to ensure data accuracy [45]. Each node cycled between sleep and data collection modes

to preserve power. Irrigation scheduling was optimized using WSN data, revealing that longer irrigation schedules, commonly used by farmers, often exceeded water requirements without improving yield, especially because the grass around the trees competed more for water in shallower soil layers [45].

In a smaller-scale deployment covering 400 m^2, a cluster-based WSN was used with only 10 nodes, some equipped with Dual-Probe Heat Pulse (DPHP) sensors for measuring moisture via a heat pulse method [46]. These nodes primarily operated in sleep mode, with scheduled wake-up cycles occurring every four days. They utilized algorithms such as the shortest path tree (SPT) and Dijkstra's algorithm for efficient data routing, while dynamically adapting to the addition or removal of nodes in the network structure. The setup emphasized energy conservation as a primary design objective, with the power draw of the DPHP sensors emerging as a major constraint [46].

Some WSN-based systems have focused more directly on automating irrigation. For example, a solar-powered, portable unit was built with a feedback-based controller designed for use in orchards of dwarf cherry trees. The goal was to reduce water stress and salinization while being affordable enough for independent growers. Three components: sensor units, valve units, and base station units, communicated wirelessly to decide when and how to irrigate based on 20 cm-deep Decagon sensor readings [47].

Another implementation explored a group-based WSN used for precision agriculture in citrus orchards. Sensors with coils operating around 93 kHz were used to monitor water content, and nodes communicated in a hierarchical, layered network. Edge computing played a key role, allowing sensors and actuator nodes to process data and make decisions locally. Based on sensor data, different irrigation actions were triggered depending on whether the entire field or only

specific zones required water. Near-ground receiver deployment was found to provide the best RSSI signal strength, particularly in areas with dense tree cover [48].

Lastly, one study proposed combining remote sensing data with WSN output through an extended Kriging interpolation method that included not only spatial coordinates but also spectral variables like Normalized Difference Vegetation Index (NDVI) and albedo [49]. The system accounted for the inherent limitations of WSNs and how remote sensing could only capture data during overpasses. Due to cloud interference, they were only able to make use of clear-sky images, and sensor noise in the WSN sometimes required smoothing and noise reduction to maintain accuracy. A leave-one-out cross-validation was used to verify interpolation results, and the method performed better when the correlation between auxiliary and target variables was weak, and often the case with spatially variable soil moisture patterns [49].

3.3 IN-SITU SOIL MONITORING TECHNIQUES

In-situ measurements play a crucial role in validating remote soil moisture sensing, such as satellite and wireless products, especially when it comes to improving accuracy through reliable ground-truth data. Recent work has focused on developing affordable sensors, evaluating placement strategies, and understanding how well point-based measurements represent larger field conditions [50]. One research study discussed the Smart Soil Sensor for Hydrology and Land Applications (SHOOL)**,** a compact, in-house device designed to measure the dielectric constant, conductivity, moisture, and temperature of soil [51]. It connects to a smartphone app for easy data visualization and note-taking. Compared to commercial probes, SHOOL showed minimal bias and a low RMSE of 2.94, offering a cost-effective option for building dense sensor networks [51]. Another study evaluated long-term fixed FDR sensors at two agricultural fields to see how well they represented average soil moisture. It turned out that some sensors that were

near the field edges were more variable and less reliable due to the different surface and subsurface conditions. The authors emphasized the need for better placement strategies or scaling methods to improve representativeness [52].

Large-scale validation efforts have also used in-situ data to assess satellite products such as the ASCAT Soil Wetness Index. Across three sites in central Italy, ASCAT-derived values showed high correlation with both in situ measurements and model simulations. Even though ASCAT has coarse resolution (25 km), the consistent temporal patterns were promising for broader applications [53]. Portable electromagnetic (EM) sensors are another useful tool for soil moisture sensing, for frequent or mobile measurements. A field study comparing 16 different EM probes found that all met the accuracy requirements after soil-specific calibration. These tools are non-invasive and flexible across various soil types, but only if they are calibrated prior to each soil type [54].

A broader review compared techniques like time-domain reflectometry (TDR) probes, capacitance sensors, and gravimetric sampling. While gravimetric methods are the most accurate, they're not practical for continuous use. TDR and capacitance sensors offer real-time data but can vary depending on soil type and sensor setup. A field comparison of four commonly used soil moisture sensors in Swiss agricultural settings demonstrated how real-world performance can present significant differences from what lab results might suggest. It showed that factors, such as environmental changes and soil texture, can substantially impact a sensor's reliability and sensitivity over time [55]. Another laboratory study examined low-cost capacitive and resistive sensors. Capacitive types performed better overall, but both types required extensive calibration to get meaningful results. Their low cost makes them appealing for large-scale monitoring, where traditional sensors may be too expensive [56].

Chapter 4. OBJECTIVE AND APPROACH

4.1 OBJECTIVE

The goal of this work is to present a non-invasive soil moisture sensing system that can accurately estimate the volumetric water content (VWC) of the top layer of soil using visible light polarization (VLP) imaging. This is achieved by combining VLP with a CNN algorithm to predict soil moisture from a single polarization channel. The system uses a linearly polarized camera to measure the polarization properties of light reflected from the soil. All of the images are collected using a Vertical-Vertical (VV) polarization orientation channel. The features that are focused on in this work are the DoLP and AoLP extracted from each image. These features capture the pixel-level variations in light scattering behavior that relate to soil texture and moisture content.

4.2 APPROACH

A first-principle approach, based on the physics of polarized light and soil reflectance, was used to perform an empirical analysis of the relationship between soil moisture and polarization parameters. Unlike satellites or radar systems that rely on multi-channel or capturing images from high altitudes, this approach uses VV single polarization to capture changes in the reflectance of the moist soil surface, as it is useful for studying natural surfaces like soil and water. The optical system captures linearly polarized light using a microgrid polarization sensor with an integrated polarization filter array (see Figure 3). Each 2×2 block of pixels corresponds to one spatial location and contains light intensity measurements at four polarization angles (0 °, 45 °, 90 °, 135 °) as shown in Figure 3. The angles are used to compute the DoLP that indicates the strength of the light that is polarized, and the AoLP that indicates the direction from which

the polarized light is coming [26]. Both of these descriptors are affected by soil moisture because of how the surface wetness affects the way light is reflected, making them the ideal features for modeling soil conditions [57].

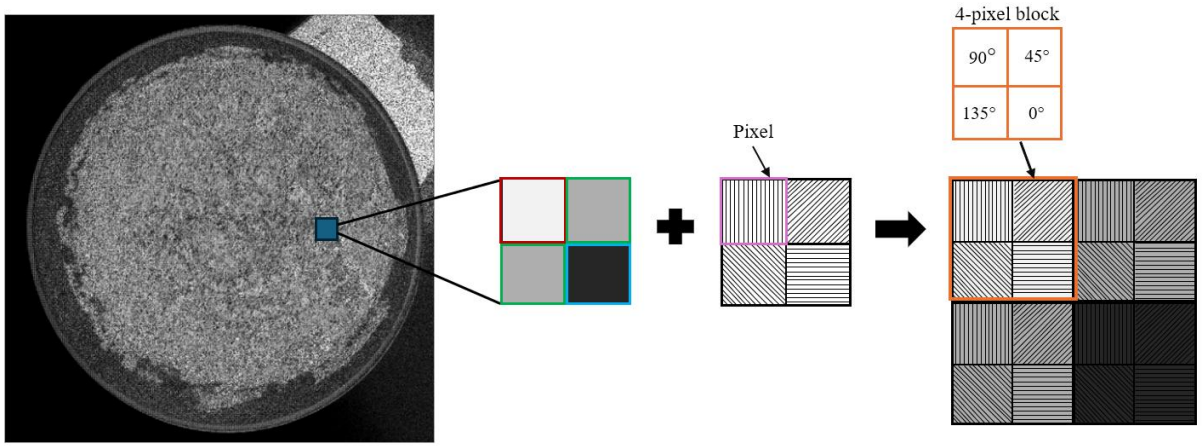

Figure 3. A 4-pixel block allows for the detection of all linear angles of polarized light by comparing the rise and fall in intensities transmitted between each pixel in the 4-pixel block.

The principle behind Brewster's angle was used to position the camera and lighting for the setup seen in Figure 4. Brewster's angle creates a zero-reflection angle where a parallel-polarized light is completely transmitted [58]. Although this angle was not explicitly calculated in the experiment, the setup was arranged based on this principle to reduce unwanted reflections. By angling the camera and the light source, the system could capture the polarization signal impacted by surface moisture without the interference from directly reflected glare. Before training, the images were cropped to a region of interest to isolate the surface of the soil and then resized to 224 × 224 pixels. The images were grouped into 15 channel composites, made up of three views captured over time, with five polarimetric slices per view based on the different lighting conditions.

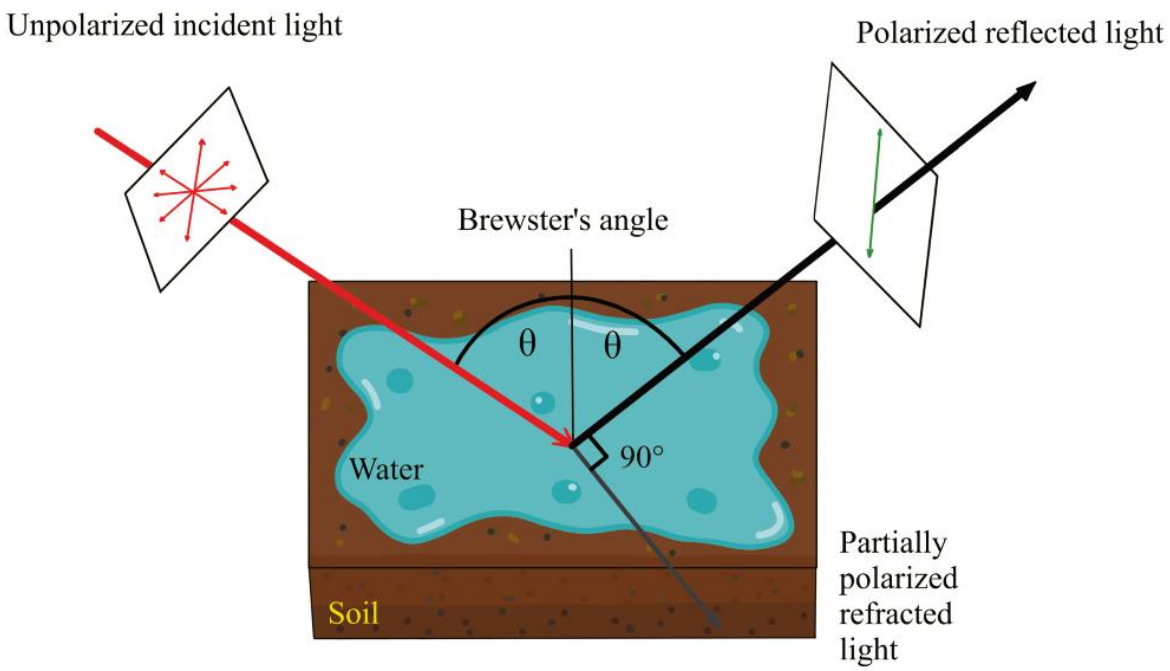

Figure 4. Light reflecting off a wet soil surface at Brewster's angle becomes polarized, enabling surface moisture detection through polarimetric imaging.

To capture the changes over time, each group of images was paired with a corresponding ground-truth moisture reading, using a capacitive soil sensor. The timestamps in the filenames were used to align each group of images with its sensor data, using a two-minute tolerance window. The resulting data was split into 75% training and 25% testing sets. The CNN structure consists of three convolution blocks with increasing filter sizes, followed by a fully connected layer, a dropout layer to reduce overfitting, and a final regression output layer to predict the soil moisture as % VWC. To evaluate the performance, the model was tested on both the training and test sets using several metrics. The metrics used are the Root Mean Squared Error (RMSE), Mean Absolute Error (MAE), R^2 (coefficient of determination), Mean Absolute Percentage Error (MAPE), and the explained variance.

Chapter 5. ITERATIVE DESIGN AND SENSOR VALIDATION

The initial idea for this work was to design a low-cost, scalable system to measure soil moisture using visible light polarimetry. A system that can be used by farmers or researchers without needing expensive, hard-to-maintain equipment. That meant leaning into affordable, off-the-shelf components whenever possible. However, as I started prototyping, the low-cost products (see Figure 5) came with their own set of challenges, many of which ultimately shaped how the system evolved.

5.1 EARLY SENSOR SELECTION AND EVALUATION

The initial sensor used in this work was the Arduino capacitive soil moisture sensor v1.2 [59-61]. The capacitive sensors were selected over resistive soil moisture sensors because resistive soil moisture sensors lack durability and quickly oxidize due to reactions with the soil [56, 62, 63]. The capacitive sensing was expected to provide a more stable and reliable measurement of the water content in the soil for long-term use. However, in practice, the sensor required extensive calibration and was highly sensitive to small fluctuations and environmental noise, leading to erratic and unusable readings. Determining that the Arduino capacitive sensor was not suitable for this work, the next sensor tested was a STEMMA capacitive sensor from Adafruit. While it demonstrated marginally better stability compared to the previous sensor, the readings remained inconsistent and difficult to interpret. The measured values failed to align with the observable changes in the soil's appearance during the drying process. This discrepancy was apparent during the gradual drying cycle, where the sensor lacked the resolution to capture subtle but important transitions in moisture content.

Figure 5. Early selection of SM sensors used for comparison. The Arduino capacitive sensor (far left), Adafruit STEMMA (second from left), ECOWITT wireless (center), and precision balance (right) used for gravimetric SM estimation.

5.2 TRANSITION TO WIRELESS DATA LOGGER

Following the limitations encountered with the Adafruit STEMMA sensor, I tested a moderate-cost ECOWITT GW1106 Soil Moisture Meter, which includes a GW1100 Wi-Fi Gateway and a WH51 multi-channel soil moisture sensor. This device was chosen due to its wireless capabilities and compatibility with a computer-based data logging interface provided with the product. It offered support for multiple sensor nodes, which in theory could allow for spatial comparison across different fields. However, in the laboratory setting, the ECOWITT onboard data logger had limited memory and would stop collecting data after a few days. While the device offered a more polished user interface, the reported values were often inconsistent and failed to reflect gradual changes in soil moisture. Without access to unfiltered data or customizable acquisition parameters, the sensor lacked the flexibility and resolution needed for the temporal analysis in this system.

5.3 GRAVIMETRIC ANALYSIS

To independently validate moisture readings using a more traditional method of gravimetric analysis by continuously tracking the weight of a soil sample as it dried. A digital laboratory-grade digital scale with an RS232 serial interface was used, and a script was written to log the weight data (g) in real-time. The goal was to leave the soil undisturbed on the scale while the camera captured the synchronized images every 15 minutes, to have a direct comparison between the visual changes and mass loss due to evaporation of the water from the soil.

However, after testing the digital scale, it was concluded that the scale was not designed for long-term continuous use. Unlike standard gravimetric procedures, where soil samples are removed and weighed at intervals of oven drying [64-66], the setup required the soil to remain in place for several days at a time. After an extended operation, the first scale began to freeze, produce loss of data, and eventually a calibration drift. In response to the scale's behavior, a second laboratory-grade digital scale was used, but unfortunately, even after multiple attempts at calibration, similar issues were presented within the second device.

A particular persistent problem of what I refer to as "phantom weight" was happening. After a drying cycle was completed and the dry soil was removed, the scale continued to display a non-zero residual weight. This suggested that while the scale could detect the presence of mass, it was not able to register gradual mass loss from the evaporating water. As a result, the evaporated moisture was not accurately captured in the logged measurements, despite a clear decrease in total soil mass. This discovery, combined with hardware reliability issues and the need to maintain precise camera alignment, made continuous gravimetric monitoring infeasible for this system.

5.4 SELECTION OF THE TEROS 10 IN-SITU MOISTURE SENSOR

As part of the process of identifying a more reliable and interpretable soil moisture sensing solution, I consulted directly with a representative from the METER group, a company known for its research-grade environmental sensors. During our discussions, I received the technical specifications of their available soil moisture probes. Based on the consultation, the TEROS 10 is a capacitive soil moisture sensor designed for higher precision and stability compared to the previously tested low-cost alternatives [67-69].

The TEROS 10 can estimate volumetric water content (VWC) in mineral soils across a range of 0 to 0.64 cm^3/cm^3, with a measurement accuracy of ±3%, making it suitable for agricultural and environmental applications where subtle changes in moisture need to be captured [68]. The TEROS 10 provided a better balance between affordability and performance and was ultimately integrated into the final sensing system to provide ground-truth moisture validation [69] alongside the polarization imaging setup. In the final setup, the system used a low-cost fully integrated HOBO MX2307 logger and TEROS 10 soil moisture with Bluetooth wireless data offload.

Chapter 6. SENSING SYSTEM

A convolutional neural network (CNN) was used to process the polarized soil images to design a non-invasive optical soil moisture sensing system. These images contain the subtle changes in surface reflectance and texture, which are often related to moisture content but are hard to model with traditional feature engineering methods. Unlike traditional feature engineering, CNNs can automatically extract and learn from visual patterns to predict soil moisture directly from the images [34, 70-72]. The CNN can preserve the original image structure that is important for soil moisture estimation because surface shine, texture changes, or patchiness can appear in different parts of the image depending on how the soil dries.

6.1 DATA PREPROCESSING AND IMAGE AQUISITION

The dataset used consisted of grayscale polarized images collected using a polarimetric imaging (PI) system at regular 15-minute intervals and paired with a corresponding ground-truth soil moisture measurement obtained every minute via in-situ probing. To align the image groups with the sensor readings, the image timestamps were matched to the nearest soil sensor reading within a ± 2-minute window. When there were multiple ground readings within the window, their average was used to form a regression label for that group.

Each data sample was created by overlapping 15 images consisting of five different lighting orientations from each of the three polarization formats. The three pixel formats in which the images were captured were PolarizeMono8 (polarized grayscale), PolarizedDoLP_BayerRG8 (Degree of Linear Polarization), and PolarizedAoLP_BayerRG8 (Angle of Linear Polarization). This preprocessed image had an input shape of 224×224×15. The

stacking provided multiple perspectives of the same soil surface to help the model retain key information regarding soil texture changes influenced by moisture.

All images were resized to 224×224 pixels to provide a suitable trade-off between preserving the spatial detail and reducing the model's complexity and computational load. While resizing can lead to loss of fine details, this effect was minimized by capturing the original image under well-lit, consistent lighting conditions to preserve important information about surface texture and polarizing behavior. The network focused on spatial and textural information rather than only on lighting differences.

6.2 NETWORK ARCHITECTURE

The CNN architecture was designed to map visual and polarimetric features from the input image directly to soil moisture levels (see Figure 6). The dataset was split into 75% training and 25% testing. The network begins with an input layer using a single 15-channel input. The model has three convolutional blocks, each followed by max pooling, and fully connected layers with dropout to predict the VWC of the soil. Each convolutional layer uses 3×3 kernel to scan over the image to identify local patterns like texture or surface changes related to moisture. After each convolutional layer, batch normalization was used to stabilize training and improve the model's convergence. Additionally, a ReLU activation layer that sets all negative values to zero and keeps positive values unchanged added non-linearity to the network. This allowed the model to learn moisture-related behaviors, such as how polarization behavior changes depending on whether the soil is damp, dry, cracked, crusted, or has a shiny surface.

A max pooling layer was applied after each convolutional layer to reduce the spatial size and retain only the most prominent features. In soil, these features can include sharp boundaries between the wet and dry regions or consistent textures that indicate the surface moisture state.

The model increased its depth by starting with 16 filters and increasing to 32 and 64 filters to allow the network to detect more complex and abstract patterns. This progression lets the model evolve from detecting simple contrasts and shadows to recognizing certain patchiness that only occurs when the soil is semi-moist, or when the soil's surface is shiny due to high saturation. The output of the final convolutional block was flattened and passed through a fully connected layer with 128 neurons to integrate all the spatial and polarimetric information to form a high-level understanding of the soil's moisture state. To prevent overfitting, a dropout layer with 50% dropout rate was applied during training. Finally, a single regression output node was predicting the volumetric water content (VWC) which is the ratio of water volume to soil volume and a standard metric used in soil science that provides a direct, physical measure of how much moisture is present in the soil.

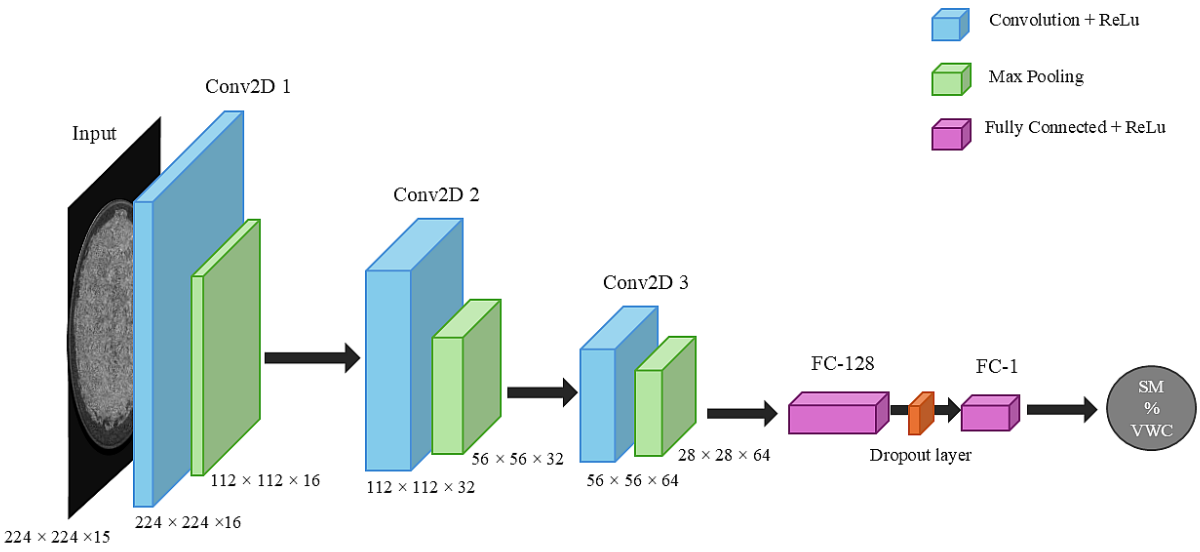

Figure 6. A convolutional neural network architecture for estimating surface soil moisture from polarized 8-bit grayscale images.

6.3 TRAINING PROCESS

The model was trained using the Adam optimization algorithm with an initial learning rate of 0.0001 for 200 epochs and L2 regularization ($\lambda = 0.001$). This extended training duration was chosen to ensure that the network had enough opportunities to converge on a stable solution and capture the underlying relationships between image features and soil moisture content. This decision was informed by empirical testing and visual monitoring of the loss curves during the training process. The training was conducted in MATLAB, utilizing automatic GPU acceleration when available, with the ground-truth labels scaled by 100 to reflect the VWC percentage. Model performance was monitored throughout training to ensure proper learning behavior and prevent overfitting.

6.4 MODEL PERFORMANCE METRICS

Performance was evaluated using multiple quantitative metrics, including the Root Mean Squared Error (RMSE), Mean Absolute Error (MAE), Mean Absolute Percentage Error (MAPE), R^2 correlation coefficient, and the explained variance score. A scatter plot comparing predicted and actual soil moisture values was also generated to visually assess prediction quality for both the training and testing sets. Additional plots showed the best-fit versus ideal identity lines to assess overestimation or underestimation trends. The results showed a high correlation between the predicted and measured values, demonstrating the model's ability to accurately estimate soil moisture by identifying the relevant image features. This method offers a promising alternative to traditional sensing methods that require direct contact with the soil.

Chapter 7. EXPERIMENTAL SETUP

The custom soil imaging and sensing station was designed to investigate the relationship between soil moisture content and the response of soil under polarized lighting (see Figure 7). To capture the images, a Triton 5.0 MP color polarization camera with a fixed focal length lens equipped with the Sony 1MX250MZR sensor was used. When positioning the soil in front of the camera, we used the ArenaView GUI to help focus and adjust the camera for a better view to capture the sample. This process was repeated for every capture cycle of 10 days. To illuminate the setup, a custom-configured 144-LED strip was arranged in a ring-like shape. The white light strip was divided into four equally sized sections, with 36 LEDs assigned to each lighting orientation to help analyze how polarized reflectance changed under different illumination conditions. Unlike traditional Pulse Width Modulated (PWM) controlled LED's, this strip was chosen for its constant current output to avoid issues with the light flickering that can occur during extended periods of time. This non-PWM lighting was important for maintaining consistent lighting across long image capture sessions.

A linear polarizing filter was positioned beneath the LED strip to ensure that the emitted light was polarized for each programmed lighting condition. To limit ambient lighting interference or reflection, the entire setup was placed inside a box that was painted with black acrylic paint. The camera was mounted to face into the enclosure, capturing images of the soil sample placed inside. Because the principle of vertical illumination from directly above generates interfering reflection on the surface, each soil-filled pot was positioned at a slight angle to ensure the camera could still capture some of the surface reflections from the moist soil to detect the effects of polarization [26, 35].

The ground truth soil moisture measurements were collected using a TEROS 10 capacitance sensor, which was inserted horizontally into the side of the pot where there was an opening to the soil, and it was approximately placed 5 cm below the soil surface. The sensor electrodes were inserted into the soil surface until they were fully covered by the soil. The sensor was connected to a data logger configured to record the Volumetric Water Content (VWC) of the soil at one-minute intervals. VWC represents the ratio of the volume of water to the total volume of soil expressed in m^3, m^{-3} or as a percentage. Based on empirical observations from the experimental cycles, a VWC of around 30 % corresponds to full saturation across all evaluated soil types. While saturation thresholds depend on the soil texture and structure, the consistent saturation threshold observed here at 30% serves as a practical reference point. The data was downloaded in bulk and exported into .xlsx and .csv files for further analysis. The setup used is seen in Figure 8.

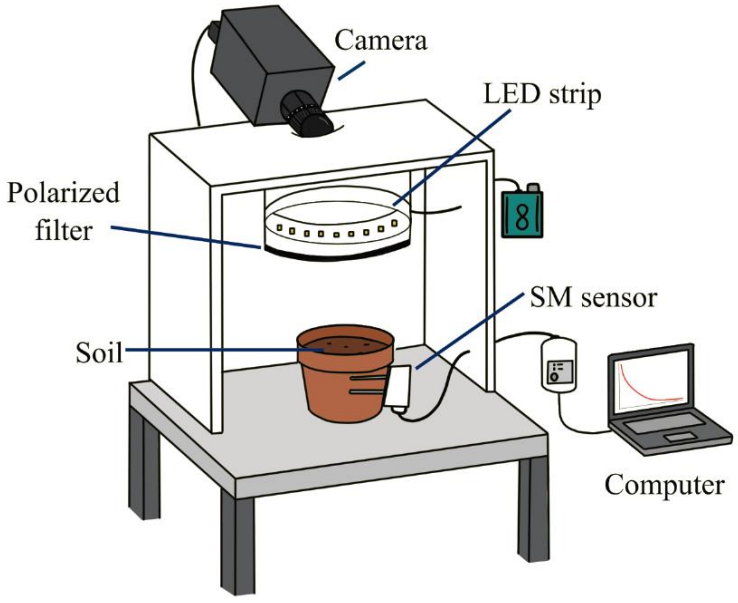

Figure 7. Simplified diagram of the setup showing a camera angled at the soil, illuminated by a polarized LED ring. A soil moisture sensor provides ground-truth data, with all components connected to a computer.

Figure 8. Experimental setup showing a soil sample placed inside a box, illuminated by a ring light with a linear polarizer. A camera is angled through a top opening to capture polarized reflectance near Brewster's angle.

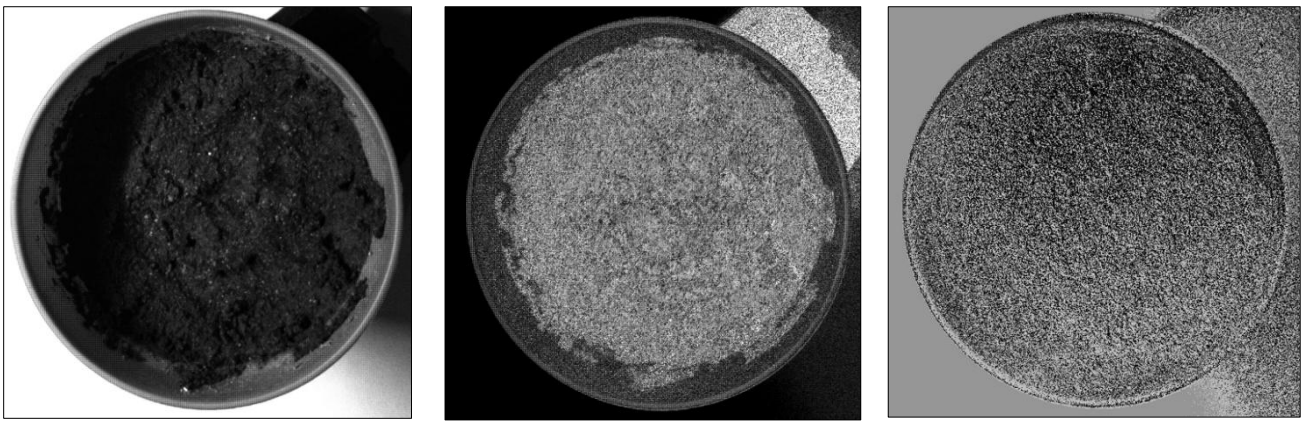

Figure 9. Pixel formats captured by the Triton polarization camera on initially moist loamy soil. From left to right: PolarizeMono8, PolarizedDolp_BayerRG8, and PolarizedAolp_BayerRG8.

The soil used in this work underwent a custom drying protocol to ensure experimental consistency. Samples were initially dried using a hotplate set to 350° Fahrenheit for one hour with minimal stirring in between for larger samples. Once dried and cooled, the soil was placed in 4-inch pots capable of holding approximately 250.31 g of content. Afterwards, ~2.37 ± 0.12 fl

oz of water was added to the soil and thoroughly mixed. Then added ~0.81 ± 0.13 fl oz of water to rinse the stirrer and ensure all soil was returned to the pot. The TEROS 10 sensor was then started for continuous soil moisture VWC data logging. A series of pilot tests was performed to determine the optimal natural drying period of the soil. Initially, we started with a one-day interval and increased the number of drying days until we established that a drying cycle of ten days was enough to achieve a consistently dry baseline before introducing water again.

The camera captured images every 15 minutes for an average cycle of 10 days. The 10 days were determined through trial runs to see how long it took for each soil sample to fully dry. For each interval, the camera captured images in three polarization pixel formats: PolarizeMono8 (greyscale), PolarizedDolp_BayerRG8 (Degree of Linear Polarization), and PolarizedAolp_BayerRG8 (Angle of Linear Polarization). These images were captured under multiple lighting directions to capture the angular dependence of polarized light reflection from the soil surface (see Figure 9).

The image and sensor readings were processed in MATLAB to extract the features relevant to soil moisture estimation. The procedure was repeated across three different soil types, sandy, organic-rich, and loamy, to evaluate the robustness of the polarization-based sensing approach across diverse soil textures and compositions (see Figure 10). These soils were collected from three different locations around the University of Washington campus. The loamy soil was collected from Sylvan Grove, and the organic-rich was collected from the Island Lane area, which had a darker color and higher moisture retention. Lastly, the sandy soil was gathered from Salmon Heming Pond, which has a finer texture and quick drying behavior.

Figure 10. Three soil types used in experiments: (left) loamy soil, (center) organic-rich garden soil, and (right) sandy soil. Each differs in texture, composition, and moisture retention properties.

Chapter 8. RESULTS

The performance of the CNN model was evaluated across twenty-three experimental cycles using five regression metrics, including the coefficient of determination (R^2), root mean squared error (RMSE), mean absolute error (MAE), mean absolute percentage error (MAPE), and the variance score. Each reported value reflects the average over twenty-three independent runs. The training and testing performance metrics across for each cycle are detailed in Table 1 and Table 2. Additionally, a comparison between two consecutive cycles using the same soil under different initial moisture conditions are shown in Table 3 and Table 4.

In Cycle 1, which used loamy soil (see Table 1 and Table 2), the model demonstrated consistently high performance. On average, the R^2 for the training dataset was 0.9865, while the testing data set resulted an R^2 of 0.9827, indicating a high correlation between the predicted and

measured VWC. These values suggest the model generalized well and was able to learn relevant visual indicators associated with moisture changes in the loamy soil. The RMSE was 0.7822% VWC for the training set and 0.8676% VWC for the testing set, reflecting the typical deviation between predicted and actual moisture levels. Similarly, the MAE values were 0.6599% VWC and 0.7374% VWC for training and testing, respectively, indicating that the average absolute error remained below one percentage point of VWC across both sets. These low error values indicate reliable predictive performance within the typical moisture range encountered during the experiment. The MAPE, which quantifies the average prediction error as a percentage of the true value, was 4.26% for training and 4.75% for testing. This metric is helpful for understanding relative error and confirms that the model maintained good accuracy even as absolute VWC values varied.

Lastly, the variance score exceeded 0.99 for both sets, further confirming that the model effectively captured most of the variability in soil moisture. Figure 11 shows the testing dataset having a high correlation between predicted and actual values, although there is some slight overfitting. Figure 12 has a higher density of data points in the (b) testing set, mainly grouping around 15-24% VWC. Figure 13 has demonstrated that the system estimates soil moisture more accurately within the 15-25% VWC range, while at extremely high and low values, the prediction accuracy decreases. These trends reflect the model's sensitivity to the visual cues of polarization and texture that change more subtly at the outer ends of the moisture spectrum.

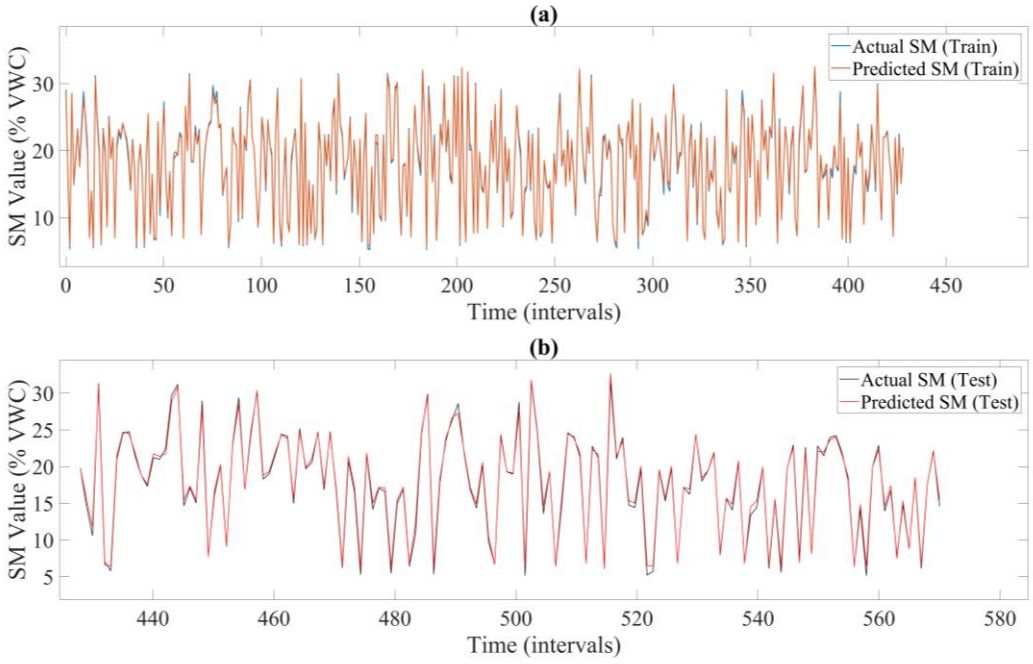

Figure 11. Predicted and actual soil moisture (% VWC) over sample order in Cycle 1 for (a) training and (b) testing data.

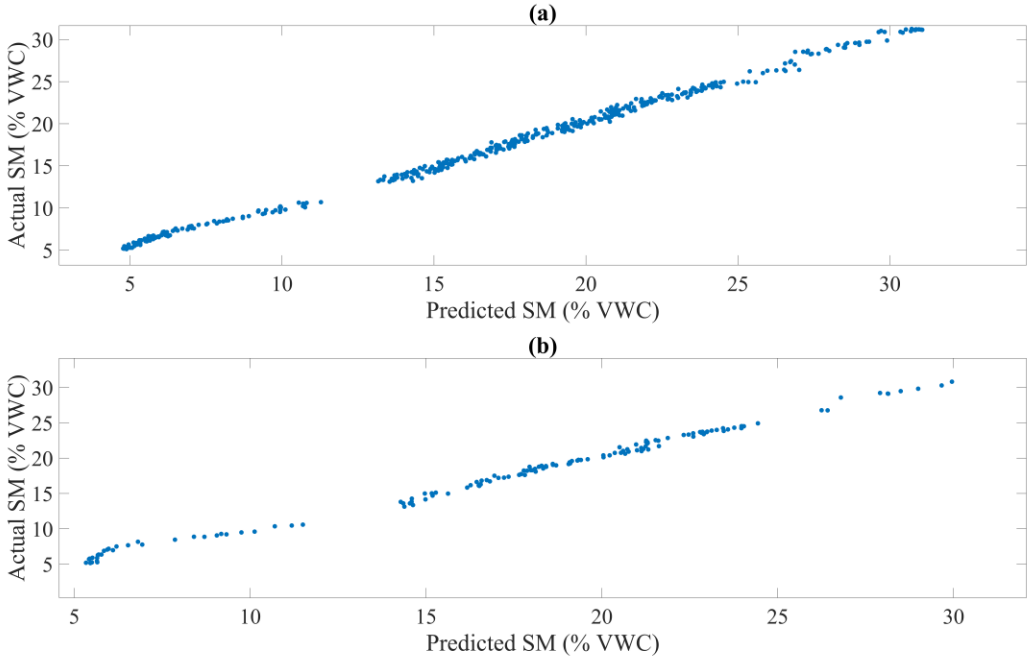

Figure 12. Scatter plots comparing predicted and actual soil moisture values (% VWC) for (a) training and (b) testing datasets for Cycle 1.

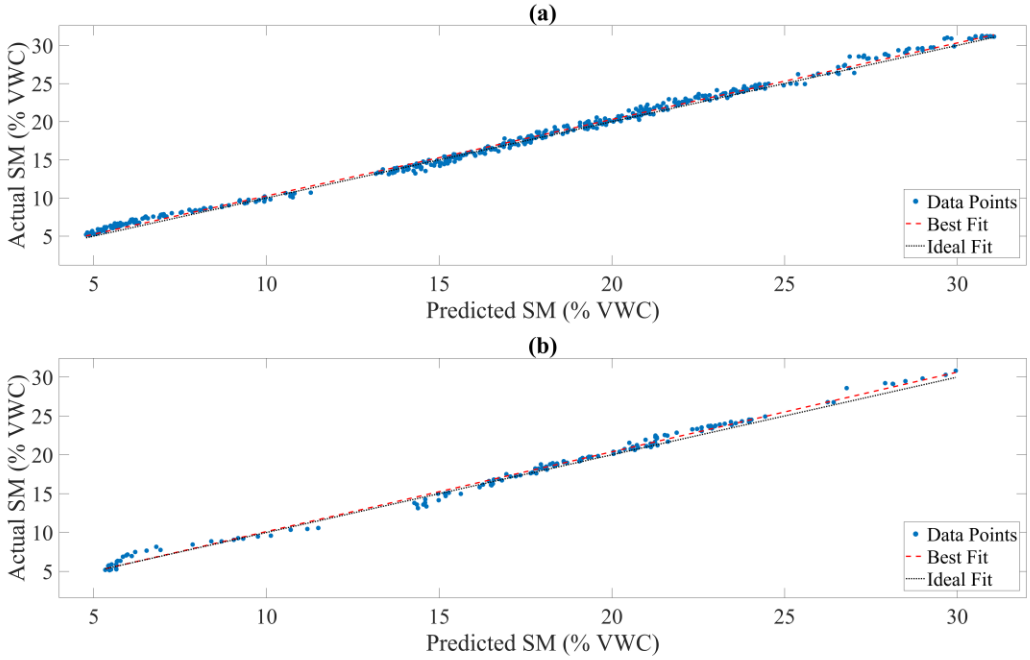

Figure 13. Comparison of predicted and actual soil moisture values (% VWC) for (a) training and (b) testing data in Cycle 1. Each plot has a best-fit line (red) and a dotted ideal 1:1 reference line (black).

In Cycle 2, the model utilized an organic-rich soil type and demonstrated generally good performance. The R^2 was 0.9714 for training, and 0.9640 for testing, indicating that the model was able to capture most of the variations in the soil moisture data. These values show that the CNN was able to make accurate predictions with the organic-rich soil that typically has greater variability in composition, surface texture, and water holding capacities. The RMSE was slightly elevated, at 0.8519% VWC for training and 1.002% VWC for testing. Similarly, the MAE was 0.7493% VWC and 0.8006% VWC for training and testing, respectively. These values suggest the model maintained an average prediction error of less than one percent VWC, although with a small increase in error compared to the more uniform loamy soil. The MAPE, which describes the error relative to the actual moisture value, was 5.39% during training and 5.63% during testing. Considering the small increases, the model's variance scores remained high at 0.9931 and 0.9854, for training and testing, respectively. These errors may reflect greater variability in surface features or inconsistencies introduced by the soil's organic composition.

In Figure 14, the training data shown in (a) maintains a consistent overlap between the predicted and actual values, which indicates that the model has effectively learned temporal changes of the moisture. Meanwhile, the testing dataset in (b) shows a small deviation between the prediction and ground-truth around the rapid peaks, likely due to sudden changes in surface appearance during rehydration, such as darkening, patchy wet spots, and increased surface roughness, which can make it harder for the model to interpret moisture levels accurately. Figure 15 further support this, showing that the majority of the data points closely follow a diagonal trend, suggesting a high correlation between predicted and actual values. However, there is a noticeable gap around 9-11% and 20-22% VWC in the testing dataset where the model

underperforms as it deviated from the identity line. This gap may indicate a region where the visual features are less distinctive or where data was underrepresented during training.

Finally, in Figure 16 a best-fit line and identity line were used to see the prediction trend. While the best-fit line closely tracks the identity line in both (a) and (b) subplots, there is a slight overprediction visible at the higher moisture values in the training and testing sets suggesting a mild overprediction in wetter conditions. This trend is consistent with the behavior observed in the scatter plots and points to an area where the model could be improved with additional training data or further tuning of the model's architecture.

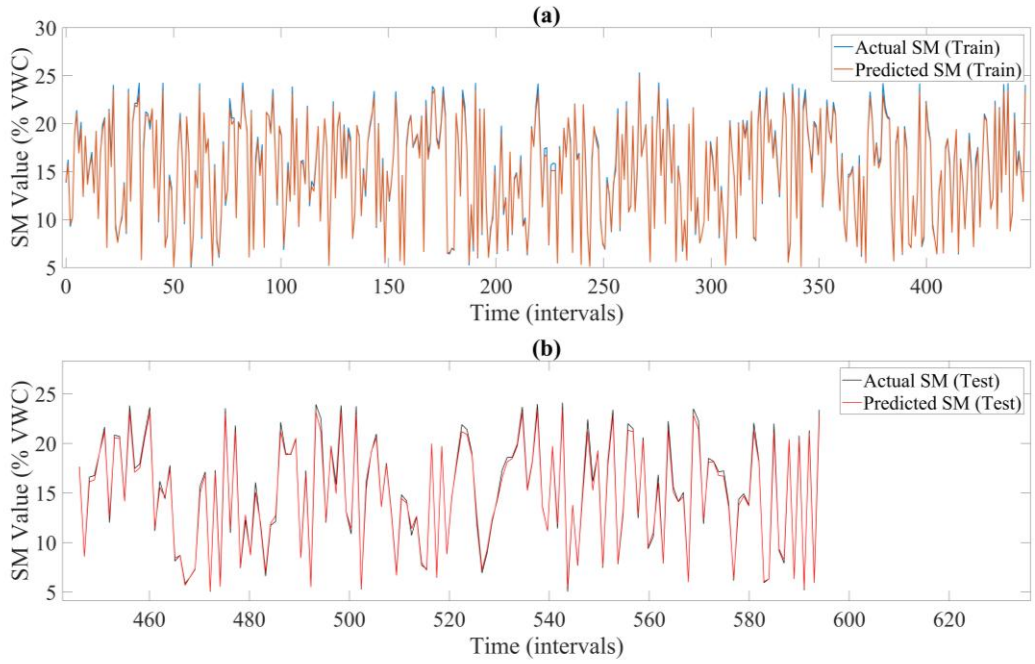

Figure 14. Predicted and actual soil moisture (% VWC) over sample order in Cycle 2 for (a) training and (b) testing data.

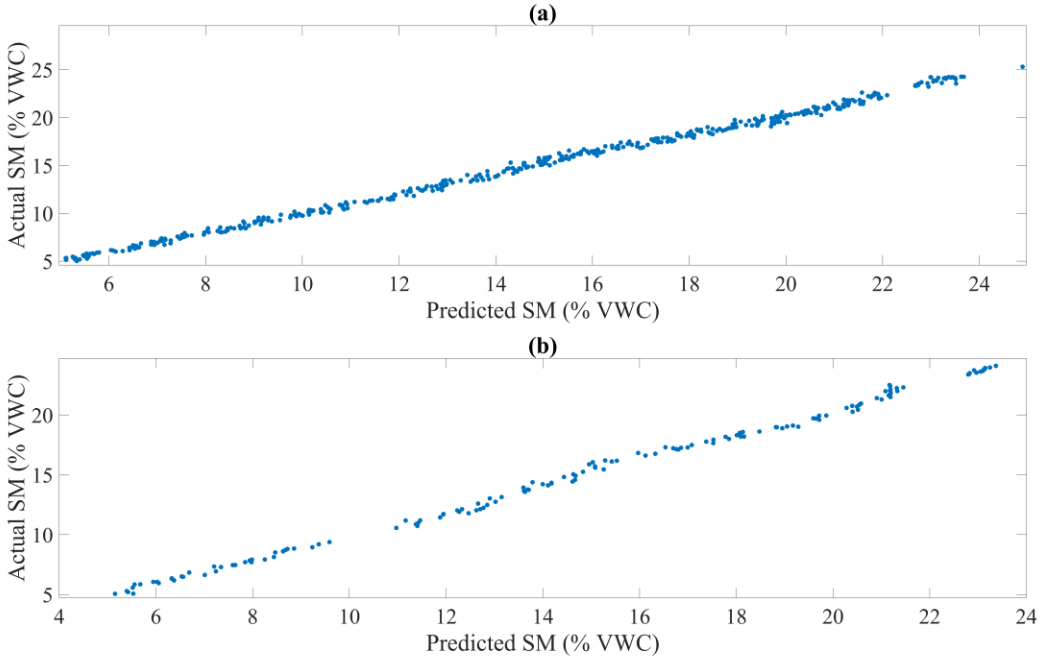

Figure 15. Scatter plots comparing predicted and actual soil moisture values (% VWC) for (a) training and (b) testing datasets for Cycle 2.

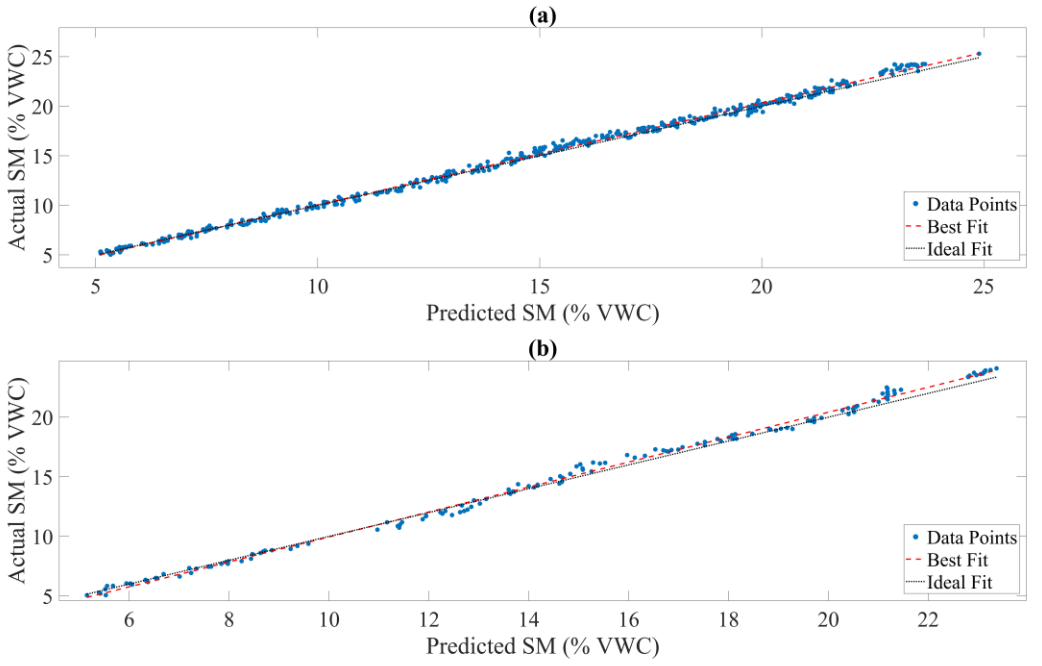

Figure 16. Comparison of predicted and actual soil moisture values (% VWC) for (a) training and (b) testing data in Cycle 2. Each plot has a best-fit line (red) and a dotted ideal 1:1 reference line (black).

Table 1. Average Training Performance Metrics of Soil Moisture Estimation with Different Soil Types.

Metric	Cycle 1 (loamy)	Cycle 2 (organic-rich)	Cycle 3 (organic-rich)	Cycle 4 (sand)
R^2	0.9865	0.9714	0.9796	0.9818
MAPE (%)	4.2626	5.3882	5.4952	4.2734
Variance	0.9945	0.9931	0.9899	0.9919
RMSE (%)	0.7822	0.8519	0.6477	0.8776
MAE (%)	0.6599	0.7493	0.5177	0.7096

Table 2. Average Testing Performance Metrics of Soil Moisture Estimation with Different Soil Types

Metric	Cycle 1 (loamy)	Cycle 2 (organic-rich)	Cycle 3 (organic-rich)	Cycle 4 (sand)
R^2	0.9827	0.9640	0.9471	0.9796
MAPE (%)	4.7478	5.6321	7.0739	4.5104
Variance	0.9919	0.9854	0.9558	0.9903
RMSE (%)	0.8676	1.0023	1.0442	0.9286
MAE (%)	0.7274	0.8006	0.7888	0.7500

For Cycle 3, the organic-rich soil used in Cycle 2 was reused to capture Cycle 3 without re-drying, as the VWC at the end of Cycle 2 was already minimal. This was intended to evaluate the repeatability of the imaging setup and the model's stability under conditions that closely

mimic real-world natural soil conditions in field applications. As a result, the soil in Cycle 3 was likely more settled and retained some surface patterns from the previous cycle, such as smoother texture, uniform darkening, or residual wet spots. These consistent visual signs may have made it easier for the model to learn and predict soil moisture more accurately. The soil resulted in the model's training performance improving compared to that of Cycle 2 (see Table 3). The R^2 increased to 0.9796, showing a slightly better correlation between the predicted and actual moisture values. The RMSE decreased from 0.8519% VWC in Cycle 2 to 0.6477% VWC, and MAE decreased from 0.7493% VWC to 0.5177% VWC, demonstrating better average accuracy. However, the MAPE increased slightly to 5.4952%, suggesting that the model may have become more sensitive to prediction errors at lower moisture levels, where small differences can lead to larger relative errors.

The testing performance also showed a similar improvement (see Table 4), with the R^2 dipping sliglight from 0.9640 in Cycle 2 to 0.9471 in Cycle 3. The RMSE also decreased from 1.0023% VWC to 1.0442% VWC, and the MAE dropped from 0.8006% VWC in Cycle 2 to 0.7888%. However, the MAPE increased to 7.0739%, likely because of the increased sensitivity to lower SM values. Even so, the variance score in the training and testing was above 0.95, meaning the model was still able to account for most of the changes in soil moisture across the datasets.

Figure 17 shows that in the training and testing data sets, the model was able to closely track the changes in the soil moisture content and Figure 18 shows that the majority of the data points are grouped around 6% and 10% VWC with only a few points near the higher moisture levels that contributed to a reduced performance at those extremes. Figure 19 demonstrates how

the predictions generally follow the ideal line in both datasets. However, there is a slight overestimation in the testing set values greater than 10% VWC (see Figure 20).

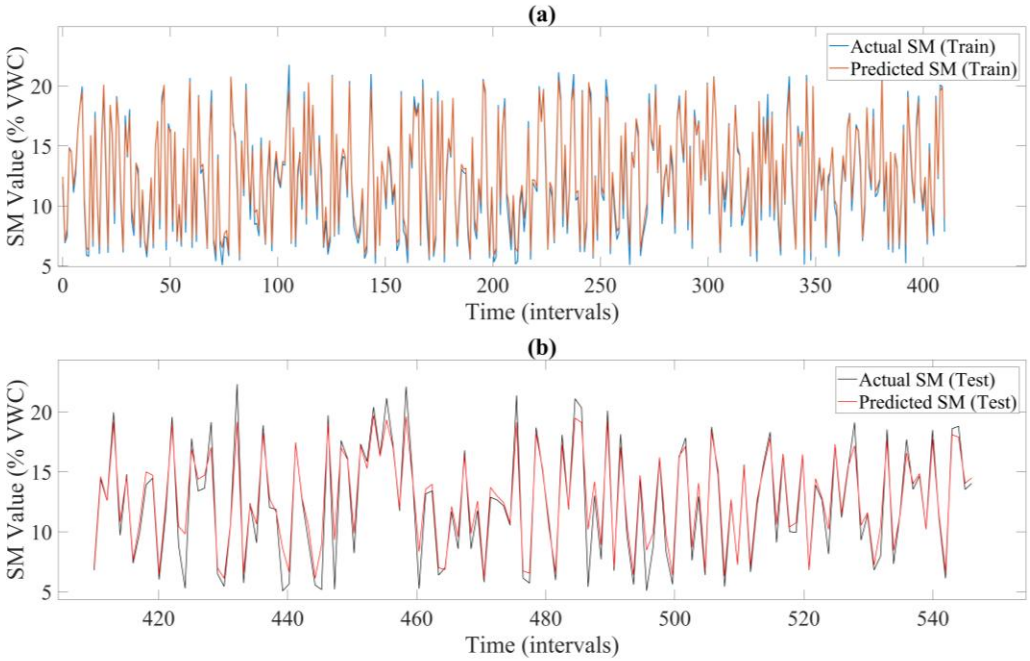

Figure 17. Predicted and actual soil moisture (% VWC) over sample order in Cycle 3 for (a) training and (b) testing data.

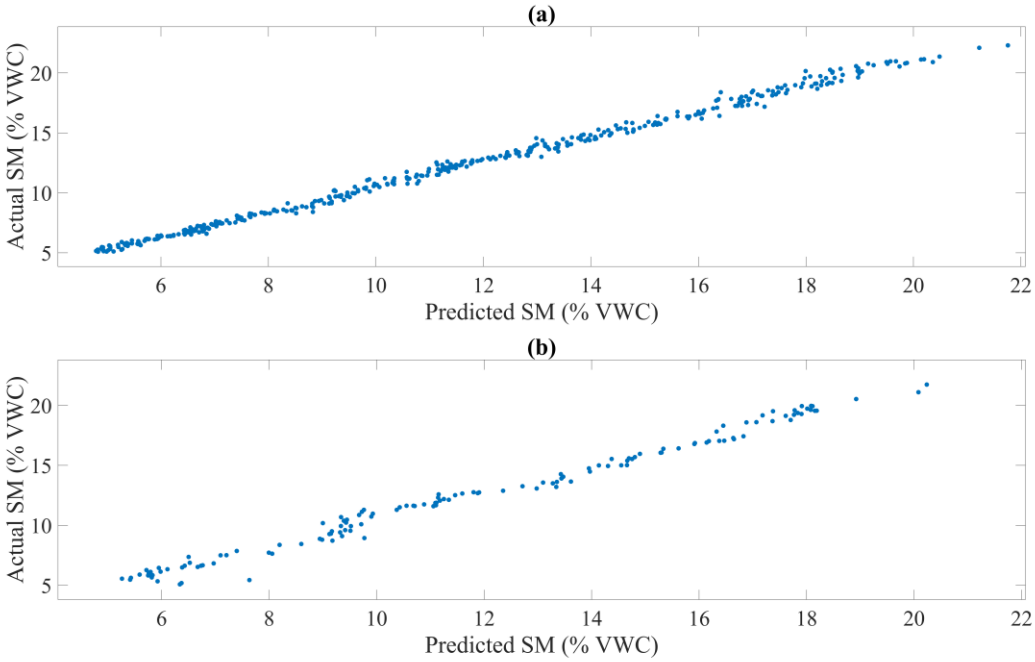

Figure 18. Scatter plots comparing predicted and actual soil moisture values (% VWC) for (a) training and (b) testing datasets for Cycle 3.

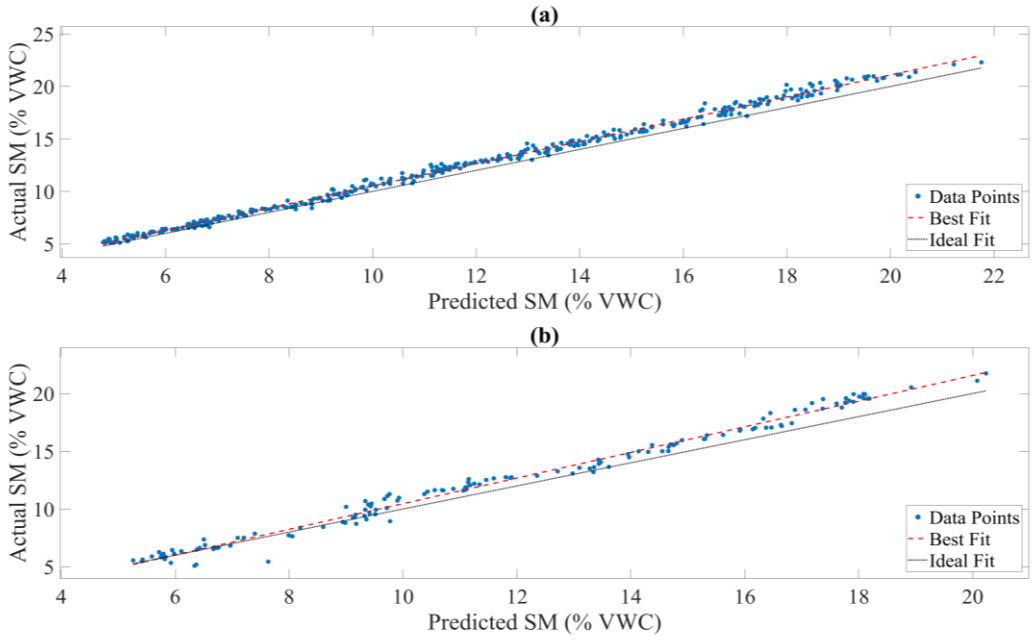

Figure 19. Comparison of predicted and actual soil moisture values (% VWC) for (a) training and (b) testing data in Cycle 3. Each plot has a best-fit line (red) and a dotted ideal 1:1 reference line (black).

Table 3. Average Training Performance on Two Consecutive Cycles with the Same Organic-Rich Soil.

Metric	Cycle 2	Cycle 3
R^2	0.9714	0.9796
MAPE (%)	5.3882	5.4952
Variance	0.9931	0.9899
RMSE (%)	0.8519	0.6477
MAE (%)	0.7493	0.5177

Table 4. Average Testing Performance on Two Consecutive Cycles with the Same Organic-Rich Soil.

Metric	Cycle 2	Cycle 3
R^2	0.9640	0.9471
MAPE (%)	5.6321	7.0739
Variance	0.9854	0.9558
RMSE (%)	1.0023	1.0442
MAE (%)	0.8006	0.7888

The previous Cycles 1, 2, and 3 were collected on loamy and organic-rich textures that have a higher water holding capacity. Cycle 4 was conducted using a sandy soil type that retains less water due to its larger particle size and minimal organic content. However, the model still

maintained a high predictive accuracy on the sandy soil as well (see Table 1 and Table 2) demonstrating a good generalization across different soil textures. The R^2 values were 0.9818 for training, and 0.9796 for testing, representing a highly reliable correlation between the predicted and the ground-truth soil moisture values on both data sets. The training errors were within an acceptable range, with an RMSE of 0.8776% VWC and 0.9286% VWC for training and testing, respectively. While the MAE in the training was 0.7096% VWC increased to 0.7500% VWC reflecting low average error and a stable predictive accuracy. Interestingly, the MAPE in the testing was slightly lower than the training set, which may reflect the reduced visual changes in the sandy soil's surface under drier conditions. The CNN system performed well in the training and testing data sets over time, with minor fluctuations during the sharper transitions (see Figure 20). The scatter plots for Cycle 4 show that the model was consistent overall, although there are fewer data points in the 25-28% VWC range (see Figure 21) which may have limited prediction accuracy at higher saturation. In Figure 22, although the data points follow the best-fit line closely, there is a noticeable dip in values below the identity line around the 16-18% VWC range.

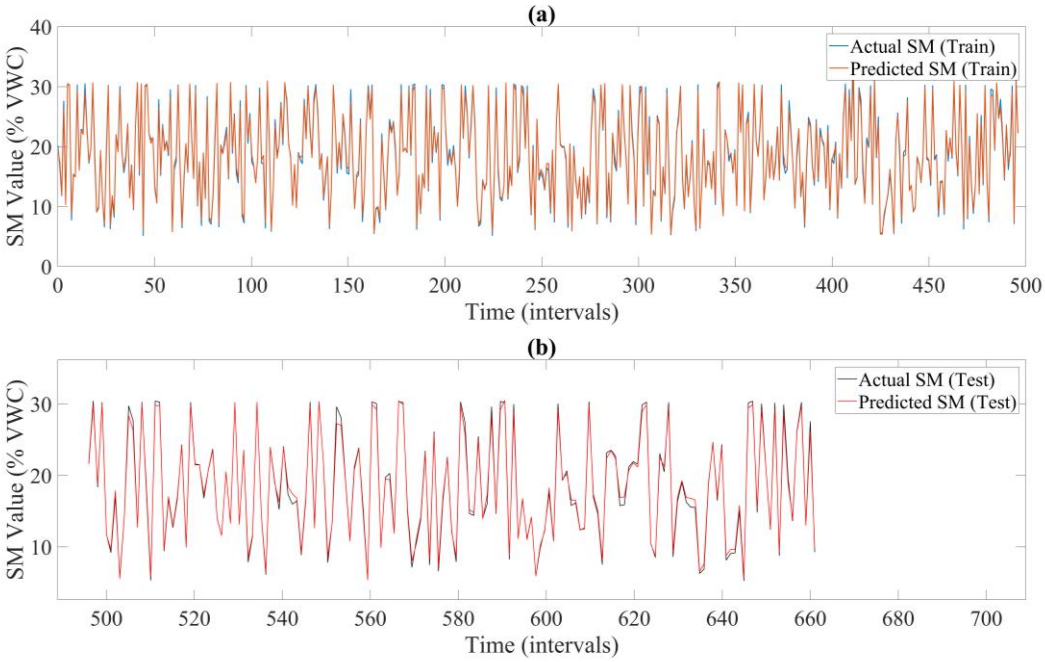

Figure 20. Predicted and actual soil moisture (% VWC) over sample order in Cycle 4 for (a) training and (b) testing data.

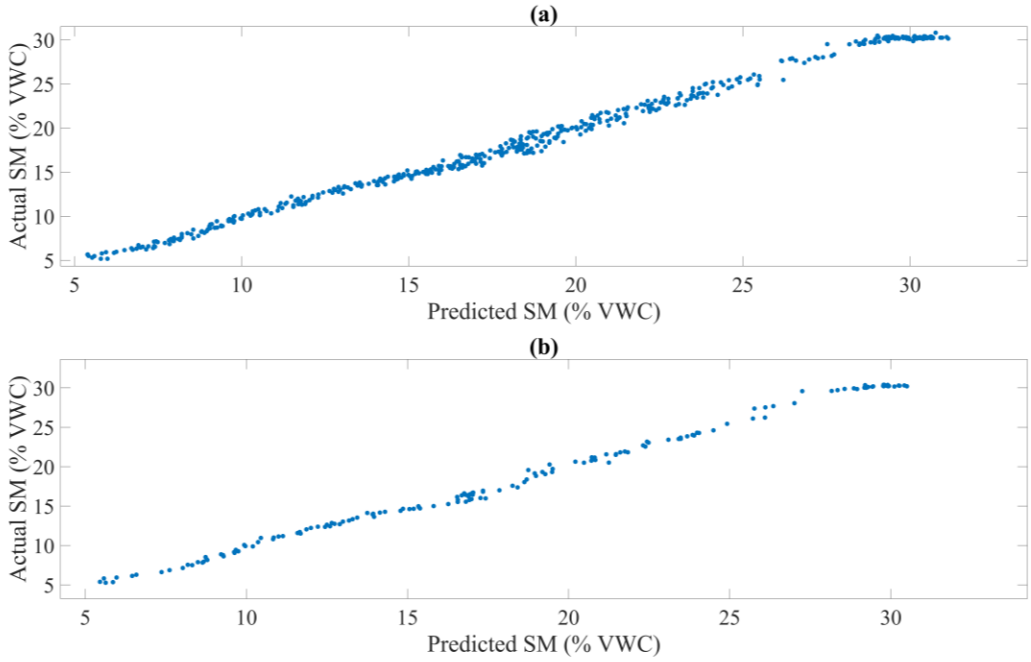

Figure 21. Scatter plots comparing predicted and actual soil moisture values (% VWC) for (a) training and (b) testing datasets for Cycle 4.

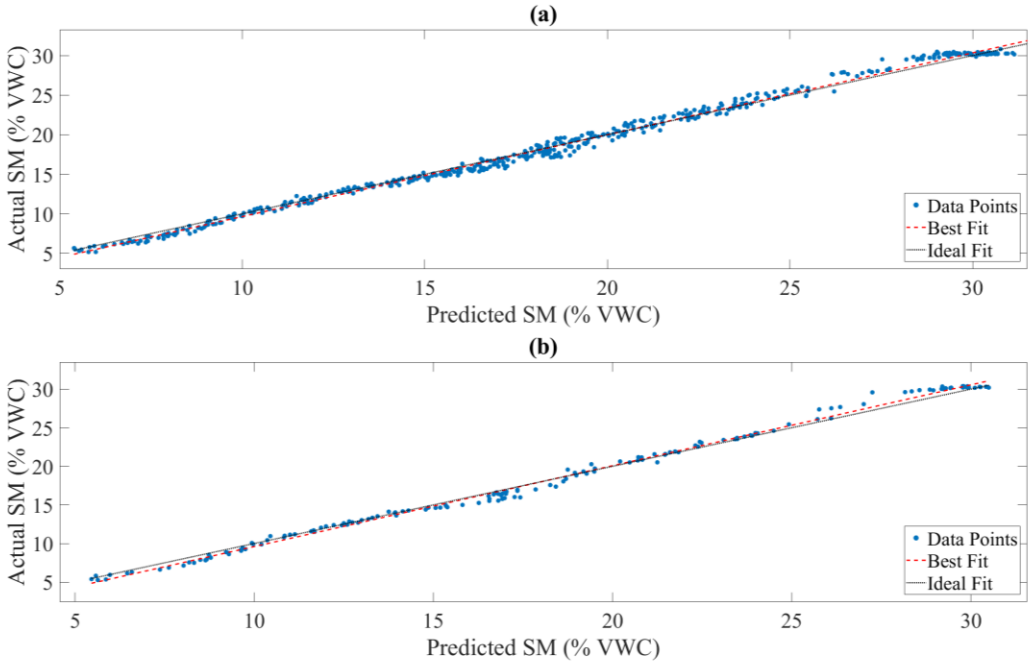

Figure 22. Comparison of predicted and actual soil moisture values (% VWC) for (a) training and (b) testing data in Cycle 4. Each plot has a best-fit line (red) and a dotted ideal 1:1 reference line (black).

Chapter 9. DISCUSSION AND LIMITATIONS

The results from the experimental cycles indicate that the CNN model successfully estimated surface soil moisture from polarized grayscale images with high accuracy and low error across all evaluated metrics (see Tables 1 and 2). These results suggest that a polarized image has useful information that can be used to estimate water content without physically contacting the soil.

The loamy soil used in Cycle 1 has finer particles and moderate water retention, leading to gradual moisture transitions. This makes it difficult for the CNN model to distinguish between moderately moist and highly saturated conditions. Grayscale imaging may further contribute to this issue, as it can cause the model to perceive surface moisture as uniformly distributed. While the model detected mid-range moisture well, it struggles with lower and extreme values due to

their visual similarity in grayscale. Cycle 1 demonstrated strong overall performance (Testing MAPE = 4.7478 %) and also revealed early weaknesses in the model's ability to confidently learn distinctive visual features.

Some small discrepancies in Cycle 2 (see Figure 14) could be due to uneven drying, soil clumping, or changes in the surface texture as the soil dried. The dip in prediction accuracy observed at 9–11% VWC in Figure 15 may result from the soil transitioning from moderately moist to visibly dry, a range where the visual differences are subtle and often hard to distinguish in grayscale polarized images. This lack of clear visual signs can reduce the model's ability to separate moisture levels in that range. Additionally, a slight deviation at 22% VWC may result from the soil being too saturated for the model to detect a significant amount of water loss accurately. In Figure 16, the discrepancy may suggest that the CNN relied on features that were too specific to the training data and couldn't be generalized to new, unseen data. This is a common issue when the dataset lacks variety, certain moisture levels are overrepresented, and others are under sampled.

In Cycle 2, the soil was fully dried and rehydrated, while in Cycle 3, the same soil was reused without drying, as it retained little moisture, and water was added. Reusing the same soil helped isolate the effect of moisture and reduced the need to reset the experiment, testing the system's ability to make accurate predictions under slightly different moisture conditions, as soils in the real world are rarely fully dried before being watered again. While the soil used in Cycle 3 did not undergo the drying process, there is still a decent accuracy (MAPE = 7.07%) in the testing set when estimating the surface soil moisture.

To evaluate soil variety, the final cycle used sandy soil, which has the largest particle size, causing it to drain and dry faster compared to the finer soils from previous cycles that retain

water for longer periods. Cycle 4 was designed to test the system's ability to detect moisture changes in soil with a faster rate of water loss. Due to its larger particle size and faster rate of water loss, the sandy soil type used in Cycle 4 allowed the model, as shown in Figure 18, to better identify key shifts in moisture levels than the models for finer soils. The testing MAPE for Cycle 4 was 4.5104%, slightly higher than that of the loamy soil in Cycle 1 and noticeably greater than the organic-rich soils used in Cycles 2 and 3. In other cycles, those soils retained water for longer, which made it challenging for the system to capture intermediate moisture values. This is further illustrated in Figure 21, where the data points for sandy soil are more evenly distributed with no significant gaps between values.

Some challenges were presented during the development of this research, each contributing to improvements in both approach and implementation. Early on, the limited background in soil science made it challenging to interpret the sensor data with confidence, as each sensor had produced unreliable or unusable values that couldn't be translated into actual moisture content. Although the sensing system was successfully assembled, the initially used low-cost sensors did not provide reliable soil moisture readings for different moisture conditions. In an effort to address this issue, I consulted with a professor from the College of Environmental Engineering at the University of Washington, who introduced me to gravimetric analysis as a more accurate method for determining ground-truth soil moisture. While this method offered improved accuracy, it was not suitable for the experiments, as it could only provide discrete measurements rather than real-time, continuous readings. To overcome the challenges with the previous setups, I contacted a representative from METER about their reputable sensors and data loggers. After extensive research, a HOBO Data Logger with a TEROS 10 METER soil moisture sensor was used due to its high accuracy and usability in smaller laboratory experiments. The

system significantly improved reliability, and data collection was restarted using this upgraded setup.

Another limitation involved the operation of the polarimetric camera, which required significant calibration and troubleshooting to ensure dependable performance. External factors, such as ambient indoor lighting and reflections from surrounding surfaces, initially impacted the consistency of the captured images. Without proper isolation of external light sources, the camera's ability to capture accurate polarization effects was compromised. To address this, I built an enclosure to block out ambient light, which reduced variability and improved image consistency. However, this process involved extensive trial and error over multiple testing sessions to establish a stable workflow. Additionally, the optimal camera height was crucial. While close-up images might seem ideal, the goal was to replicate a practical scenario where a person holds the camera at a reasonable distance from the soil. As such, the camera was positioned at a height of approximately two feet to simulate this real-world setup. Despite the challenges, these adjustments ultimately contributed to a more reliable experimental design and improved the overall results.

Chapter 10. CONCLUSION

This work presented the successful development, evaluation, and implementation of a soil moisture estimation system using visible light polarimetry (VLP), motivated by the need for a high-resolution, non-invasive soil moisture monitoring tool. The study investigated the feasibility of using polarization-sensitive imaging as an alternative to traditional in-ground sensing methods. Through iterative prototyping and sensor testing, the limitations of commonly available low-cost capacitive and wireless soil moisture sensors became evident. The initial attempts to use

Arduino-based and STEMMA Adafruit sensors, along with the wireless data logger, presented challenges in stability and interpretability due to slow evaporation cycles. Additionally, gravimetric methods using laboratory-grade weight scales were attempted to track mass loss, and further converting to volumetric water content was not successful. Technical constraints such as scale calibration drifts, system instability during continuous active use, and measurement artifacts (e.g, “phantom weight”) made long-term gravimetric validation impractical. The final system utilized a HOBO MX2307 and TEROS 10 soil moisture and temperature data logger, which has Bluetooth wireless data offload, to provide a more stable ground truth for validating the optical polarization system.

The final system utilized a Triton polarization camera with a Sony IMX250MZR sensor, capturing four polarization angles every 15 minutes to monitor the drying cycle of soil. The polarization data, processed into Degree of Linear Polarization (DoLP) and Angle of Linear Polarization (AoLP) maps, enabled surface-level sensing with spatial resolution. These images were paired with in-situ measurements to train a convolutional neural network (CNN) capable of predicting soil moisture content from visual features. The model demonstrated the ability to capture complex surface reflectance patterns that correlate with moisture levels. In the end, this work shows that when combined with machine learning, visible light polarimetry provides a powerful framework for estimating surface soil moisture.

Chapter 11. FUTURE WORK

While the current system demonstrates the validity of detecting soil moisture via VLP, further improvements can be made through the following efforts to increase the robustness and adaptability of soil moisture dynamics. For future work, it would be more beneficial to test the

system across multiple types of soil. The different soil properties, such as color, salinity, texture, and temperature, can impact the reflectance and polarization behavior. Understanding these effects can help inform the design of a more versatile sensor that is capable of operating consistently without the need to frequently recalibrate.

Additionally, to help assess its applicability in a real-world scenario where farmers and researchers in environmental management are the primary users, the system should be evaluated outdoors under dynamically changing sunlight conditions, and the impact of cloud coverage should be considered. One aspect that wasn't tested during this work was the impact of soil temperature on the moisture readings. Measuring the sensor's temperature sensitivity could help develop a temperature correction model to improve the accuracy of VWC estimates.

Another area that could potentially be investigated is scaling the system to include multiple polarization sensors positioned at different angles to capture a broader and more informative view of the soil surface. By using multiple angles instead of relying on a single stationary, polarized camera with a limited focus on a small area of soil, we can gather more information on surface texture, vegetation interference, and spatial variation in moisture. To expand more on how dense or sparse vegetation can affect the results, using all types and levels of vegetation cover in experimental setups to approximate the effects on the relationship between brightness temperature and soil moisture would be needed [73]. In addition to the different angles, mounting the system at variable heights, such as on a tripod or installed in a greenhouse with controlled lighting, could reduce the need for ground contact while expanding the coverage of the sensing area. Another future direction involves investigating the combination of other sensing techniques with VLP, such as thermal imaging and mmWave radar. These could provide surface and subsurface moisture information to build a more complete picture of what is

happening in the soil while keeping the system contact-free. This future research will help develop an adaptive sensing approach to determine how well the system performs for field deployments in dynamic and natural environments.

BIBLIOGRAPHY

[1] A. Garg, P. Munoth, and R. Goyal, "Application of soil moisture sensor in agriculture," in *Proceedings of Internation Conference on Hydraulic*, 2016, pp. 8-10.

[2] B. Kashyap and R. Kumar, "Sensing methodologies in agriculture for soil moisture and nutrient monitoring," *IEEE Access,* vol. 9, pp. 14095-14121, 2021.

[3] T. J. Jackson, "Satellite remote sensing of soil moisture," in *Advances in Water Science Methodologies, Ch.6*: CRC Press, 2005, pp. 91-96.

[4] T. J. Schmugge, "Remote sensing of soil moisture: Recent advances," *IEEE Transactions on Geoscience and Remote Sensing,* no. 3, pp. 336-344, 1983.

[5] Y. Wang *et al.*, "A Review of Earth's Surface Soil Moisture Retrieval Models via Remote Sensing," *Water,* vol. 15, no. 21, p. 3757, 2023.

[6] T. Mu, G. Liu, X. Yang, and Y. Yu, "Soil-Moisture Estimation Based on Multiple-Source Remote-Sensing Images," *Remote Sensing,* vol. 15, no. 1, p. 139, 2023.

[7] W. Xiao and Z. Zengxiang, "A review: theories, methods and development of soil moisture monitoring by remote sensing," presented at the Proceedings. 2005 IEEE International Geoscience and Remote Sensing Symposium, 2005. IGARSS '05, Seoul, Korea (South), 2005.

[8] P. J. Curran, "Remote sensing: The use of polarized visible light (PVL) to estimate surface soil moisture," *Applied Geography,* vol. 1, no. 1, pp. 41-53, 1981.

[9] H. McNairn and B. Brisco, "The application of C-band polarimetric SAR for agriculture: A review," *Canadian journal of remote sensing,* vol. 30, no. 3, pp. 525-542, 2004.

[10] M. Hardie, "Review of novel and emerging proximal soil moisture sensors for use in agriculture," *Sensors,* vol. 20, no. 23, p. 6934, 2020.

[11] H. R. Bogena, J. A. Huisman, C. Oberdörster, and H. Vereecken, "Evaluation of a low-cost soil water content sensor for wireless network applications," *Journal of Hydrology,* vol. 344, no. 1-2, pp. 32-42, 2007.

[12] J. Hrisko, "Capacitive soil moisture sensor theory, calibration, and testing," *no,* vol. 2, pp. 1-12, 2020.

[13] G. METER, "Soil moisture sensors-How they work. Why some are not research-grade," ed: July, 2020.

[14] J. Hrisko, "Capacitive Soil Moisture Sensor Calibration with Arduino," *Maker Portal. Available online: https://makersportal. com/blog/2020/5/26/capacitive-soil-moisture-calibration-with-arduino (accessed on 21 May 2019),* 2021.

[15] E. H. Hegazi, L. Yang, and J. Huang, "A convolutional neural network algorithm for soil moisture prediction from Sentinel-1 SAR images," *Remote sensing,* vol. 13, no. 24, p. 4964, 2021.

[16] A. Singh, K. Gaurav, G. K. Meena, and S. Kumar, "Estimation of soil moisture applying modified dubois model to Sentinel-1; a regional study from central India," *Remote Sensing,* vol. 12, no. 14, p. 2266, 2020.

[17] E. H. Hegazi, A. A. Samak, L. Yang, R. Huang, and J. Huang, "Prediction of soil moisture content from sentinel-2 images using convolutional neural network (CNN)," *Agronomy,* vol. 13, no. 3, p. 656, 2023.

[18] L. Ge, R. Hang, Y. Liu, and Q. Liu, "Comparing the performance of neural network and deep convolutional neural network in estimating soil moisture from satellite observations," *Remote Sensing,* vol. 10, no. 9, p. 1327, 2018.

[19] T. Jagdhuber, "Soil parameter retrieval under vegetation cover using SAR polarimetry," RIMAX Publications, RIMAX, Deutsches GeoForschungsZentrum, 2012.

[20] J. Raffoul, D. LeMaster, and K. Hirakawa, "Framework for improving DoLP and AoLP reconstruction quality in microgrid polarimeters," *Optics Express,* vol. 30, no. 26, pp. 48004-48020, 2022.

[21] F.-M. Breon, D. Tanre, P. Lecomte, and M. Herman, "Polarized reflectance of bare soils and vegetation: measurements and models," *IEEE Transactions on Geoscience and Remote Sensing,* vol. 33, no. 2, pp. 487-499, 1995.

[22] G. Hassan, K. Ismail, N. Persaud, and R. Reneau Jr, "Dependence of the degree of linear polarization in scattered visible light on soil textural fractions," *Soil science,* vol. 169, no. 11, pp. 806-814, 2004.

[23] X. Sun, J. Hong, and Y. Qiao, "Measurements of multi-angle polarization properties of the water-bearing yellow brown soil using multi-band polarimetric imagery in the laboratory," in *2008 International Conference on Optical Instruments and Technology: Optoelectronic Measurement Technology and Applications*, 2009, vol. 7160: SPIE, pp. 229-239.

[24] S. N. Savenkov, A. A. Kokhanovsky, E. A. Oberemok, and I. S. Kolomiets, "Mueller matrices of soil and vegetation in the visible range," *IEEE Geoscience and Remote Sensing Letters,* vol. 17, no. 8, pp. 1383-1385, 2019.

[25] Q. Wang, J. Sun, X. Chang, T. Jin, J. Shang, and Z. Liu, "The correction method of water and fresnel reflection coefficient for soil moisture retrieved by CYGNSS," *Remote Sensing,* vol. 15, no. 12, p. 3000, 2023.

[26] D. Murphy, K. Spring, and M. Davidson. "Introduction to Polarized Light." Nikon's MicroscopyU, The Source for Microscopy Education. https://www.microscopyu.com/techniques/polarized-light/introduction-to-polarized-light (accessed.

[27] S. Nachum, "Soil Water Potential in Geosciences: An Overview," *Geosciences,* vol. 15, no. 4, p. 123, 2025.

[28] M. Owe, R. de Jeu, and J. Walker, "A methodology for surface soil moisture and vegetation optical depth retrieval using the microwave polarization difference index," *IEEE Transactions on Geoscience and Remote Sensing,* vol. 39, no. 8, pp. 1643-1654, 2001.

[29] F. Snik *et al.*, "An overview of polarimetric sensing techniques and technology with applications to different research fields," *Polarization: measurement, analysis, and remote sensing XI,* vol. 9099, pp. 48-67, 2014.

[30] A. A. Arroyo *et al.*, "Dual-polarization GNSS-R interference pattern technique for soil moisture mapping," *IEEE Journal of Selected Topics in Applied Earth Observations and Remote Sensing,* vol. 7, no. 5, pp. 1533-1544, 2014.

[31] J. Yu, X. Zhang, L. Xu, J. Dong, and L. Zhangzhong, "A hybrid CNN-GRU model for predicting soil moisture in maize root zone," *Agricultural Water Management,* vol. 245, p. 106649, 2021.

[32] T. M. Roberts, I. Colwell, C. Chew, S. Lowe, and R. Shah, "A deep-learning approach to soil moisture estimation with GNSS-R," *Remote Sensing,* vol. 14, no. 14, p. 3299, 2022.

[33] Y. Chen *et al.*, "Convolutional neural network model for soil moisture prediction and its transferability analysis based on laboratory Vis-NIR spectral data," *International Journal of Applied Earth Observation and Geoinformation,* vol. 104, p. 102550, 2021.

[34] M. Swapna, Y. K. Sharma, and B. Prasadh, "CNN Architectures: Alex Net, Le Net, VGG, Google Net, Res Net," *Int. J. Recent Technol. Eng,* vol. 8, no. 6, pp. 953-960, 2020.

[35] A. Sivaram, L. Das, and V. Venkatasubramanian, "Hidden representations in deep neural networks: Part 1. Classification problems," *Computers & Chemical Engineering,* vol. 134, p. 106669, 2020.

[36] P. C. Dubois, J. Van Zyl, and T. Engman, "Measuring soil moisture with imaging radars," *IEEE transactions on geoscience and remote sensing,* vol. 33, no. 4, pp. 915-926, 1995.

[37] B. P. Mohanty, M. H. Cosh, V. Lakshmi, and C. Montzka, "Soil moisture remote sensing: State-of-the-science," *Vadose Zone Journal,* vol. 16, no. 1, pp. 1-9, 2017.

[38] L. Wang and J. J. Qu, "Satellite remote sensing applications for surface soil moisture monitoring: A review," *Frontiers of Earth Science in China,* vol. 3, pp. 237-247, 2009.

[39] L. Brocca *et al.*, "Soil as a natural rain gauge: Estimating global rainfall from satellite soil moisture data," *Journal of Geophysical Research: Atmospheres,* vol. 119, no. 9, pp. 5128-5141, 2014.

[40] A. Gruber *et al.*, "Validation practices for satellite soil moisture retrievals: What are (the) errors?," *Remote sensing of environment,* vol. 244, p. 111806, 2020.

[41] K. Y. Vinnikov *et al.*, "Satellite remote sensing of soil moisture in Illinois, United States," *Journal of Geophysical Research: Atmospheres,* vol. 104, no. D4, pp. 4145-4168, 1999.

[42] E. Babaeian, M. Sadeghi, S. B. Jones, C. Montzka, H. Vereecken, and M. Tuller, "Ground, proximal, and satellite remote sensing of soil moisture," *Reviews of Geophysics,* vol. 57, no. 2, pp. 530-616, 2019.

[43] B. P. Banerjee, S. Raval, and P. Cullen, "UAV-hyperspectral imaging of spectrally complex environments," *International Journal of Remote Sensing,* vol. 41, no. 11, pp. 4136-4159, 2020.

[44] R. Sui and J. Baggard, "Wireless sensor network for monitoring soil moisture and weather conditions," *Applied engineering in agriculture,* vol. 31, no. 2, pp. 193-200, 2015.

[45] B. Majone *et al.*, "Wireless sensor network deployment for monitoring soil moisture dynamics at the field scale," *Procedia environmental sciences,* vol. 19, pp. 426-435, 2013.

[46] J. John, V. S. Palaparthy, S. Sarik, M. S. Baghini, and G. S. Kasbekar, "Design and implementation of a soil moisture wireless sensor network," in *2015 Twenty First National Conference on Communications (NCC)*, 2015: IEEE, pp. 1-6.

[47] M. Dursun and S. Ozden, "A wireless application of drip irrigation automation supported by soil moisture sensors," *Scientific Research and Essays,* vol. 6, no. 7, pp. 1573-1582, 2011.

[48] J. Lloret, S. Sendra, L. Garcia, and J. M. Jimenez, "A wireless sensor network deployment for soil moisture monitoring in precision agriculture," *Sensors,* vol. 21, no. 21, p. 7243, 2021.

[49] J. Zhang, X. Li, R. Yang, Q. Liu, L. Zhao, and B. Dou, "An extended kriging method to interpolate near-surface soil moisture data measured by wireless sensor networks," *Sensors,* vol. 17, no. 6, p. 1390, 2017.

[50] J. P. Walker, G. R. Willgoose, and J. D. Kalma, "In situ measurement of soil moisture: a comparison of techniques," *Journal of Hydrology,* vol. 293, no. 1-4, pp. 85-99, 2004.

[51] H. Agrawal *et al.*, "Performance evaluation of a newly in-house developed in-situ soil moisture sensor with standard industrial sensors and gravimetric sampling," *Journal of Geomatics,* vol. 13, no. 2, pp. 280-284, 2019.

[52] G. C. Heathman, M. H. Cosh, E. Han, T. J. Jackson, L. McKee, and S. McAfee, "Field scale spatiotemporal analysis of surface soil moisture for evaluating point-scale in situ networks," *Geoderma,* vol. 170, pp. 195-205, 2012.

[53] L. Brocca, F. Melone, T. Moramarco, W. Wagner, and S. Hasenauer, "ASCAT soil wetness index validation through in situ and modeled soil moisture data in central Italy," *Remote Sensing of Environment,* vol. 114, no. 11, pp. 2745-2755, 2010.

[54] H. Kim, M. H. Cosh, R. Bindlish, and V. Lakshmi, "Field evaluation of portable soil water content sensors in a sandy loam," *Vadose Zone Journal,* vol. 19, no. 1, p. e20033, 2020.

[55] H. Mittelbach, I. Lehner, and S. I. Seneviratne, "Comparison of four soil moisture sensor types under field conditions in Switzerland," *Journal of Hydrology,* vol. 430, pp. 39-49, 2012.

[56] S. Adla, N. K. Rai, S. H. Karumanchi, S. Tripathi, M. Disse, and S. Pande, "Laboratory calibration and performance evaluation of low-cost capacitive and very low-cost resistive soil moisture sensors," *Sensors,* vol. 20, no. 2, p. 363, 2020.

[57] X. Li *et al.*, "Polarimetric Imaging via Deep Learning: A Review," *Remote Sensing,* vol. 15, no. 6, p. 1540, 2023.

[58] A. Lakhtakia, "Would Brewster recognize today's Brewster angle," *Optics News,* vol. 15, no. 6, pp. 14-18, 1989.

[59] P. Placidi, L. Gasperini, A. Grassi, M. Cecconi, and A. Scorzoni, "Characterization of low-cost capacitive soil moisture sensors for IoT networks," *Sensors,* vol. 20, no. 12, p. 3585, 2020.

[60] F. Kizito *et al.*, "Frequency, electrical conductivity and temperature analysis of a low-cost capacitance soil moisture sensor," *Journal of Hydrology,* vol. 352, no. 3-4, pp. 367-378, 2008.

[61] I. M. Kulmány *et al.*, "Calibration of an Arduino-based low-cost capacitive soil moisture sensor for smart agriculture," *Journal of Hydrology and Hydromechanics,* vol. 70, no. 3, pp. 330-340, 2022.

[62] S. Chowdhury, S. Sen, and S. Janardhanan, "Comparative analysis and calibration of low cost resistive and capacitive soil moisture sensor," *arXiv preprint arXiv:2210.03019,* 2022.

[63] M. Saleh, I. H. Elhajj, D. Asmar, I. Bashour, and S. Kidess, "Experimental evaluation of low-cost resistive soil moisture sensors," in *2016 IEEE International Multidisciplinary Conference on Engineering Technology (IMCET)*, 2016: IEEE, pp. 179-184.

[64] C. Montzka *et al.*, "Soil moisture product validation good practices protocol," 2021.

[65] M. Maltz, E. Aronson, K. Arogyaswamy, and N. Rodriguez, "Gravimetric Soil Moisture X-CZO, Modified from KBS-LTER, as per Robertson et al. 1999," 2019.

[66] A. Shukla *et al.*, "Soil moisture estimation using gravimetric technique and FDR probe technique: a comparative analysis," *American International Journal of Research in Formal, Applied & Natural Sciences,* vol. 8, no. 1, pp. 89-92, 2014.

[67] A. Fragkos, D. Loukatos, G. Kargas, E. Symeonaki, and K. G. Arvanitis, "Assessment of the TEROS 10 and TEROS 12 sensors in soil moisture measurement," in *E3S Web of Conferences*, 2024, vol. 551: EDP Sciences, p. 03005.

[68] A. Fragkos, D. Loukatos, G. Kargas, and K. G. Arvanitis, "Performance Evaluation of TEROS 10 Sensor in Diverse Substrates and Soils of Different Electrical Conductivity Using Low-Cost Microcontroller Settings," *Land,* vol. 14, no. 2, p. 242, 2025.

[69] S. Cominelli, L. D. Rivera, W. G. Brown, T. E. Ochsner, and A. Patrignani, "Calibration of TEROS 10 and TEROS 12 electromagnetic soil moisture sensors," *Soil Science Society of America Journal,* vol. 88, no. 6, pp. 2104-2122, 2024.

[70] Y. Wang, L. Shi, Y. Hu, X. Hu, W. Song, and L. Wang, "A comprehensive study of deep learning for soil moisture prediction," *Hydrology and Earth System Sciences Discussions,* vol. 2023, pp. 1-38, 2023.

[71] S. Saha, "A comprehensive guide to convolutional neural networks—the ELI5 way," *Towards data science,* vol. 15, p. 15, 2018.

[72] E. Malach and S. Shalev-Shwartz, "Computational separation between convolutional and fully-connected networks," *arXiv preprint arXiv:2010.01369,* 2020.

[73] Y.-A. Liou, S.-F. Liu, and W.-J. Wang, "Retrieving soil moisture from simulated brightness temperatures by a neural network," *IEEE Transactions on Geoscience and Remote Sensing,* vol. 39, no. 8, pp. 1662-1672, 2001.